A Source-Based Test-Bed for Fast-Neutron Irradiation

Scherzinger, Julius

2015

Licentiate Thesis

A Source-Based Test-Bed for Fast-Neutron Irradiation

by
Julius Scherzinger

Division of Nuclear Physics
Department of Physics
Lund University

20. March 2015

LUND
UNIVERSITY

A Source-Based Test-Bed for Fast-Neutron Irradiation
Licentiate Thesis

Division of Nuclear Physics
Department of Physics
Lund University
Box 118
SE-221 00 Lund
Sweden

Typeset by author using LaTeX

Abstract

The "^{3}He crisis" has resulted in a major effort worldwide to develop replacement neutron-detector technologies. Such technologies are in their infancy and need to be thoroughly tested before becoming mainstream. Neutron sources for controlled irradiation include accelerators, nuclear reactors and radioactive sources. Neutrons produced in nuclear reactors and at accelerators have a very high cost per neutron. In contrast, radioactive sources produce neutrons at a significantly lower cost per neutron and with a substantially lower cost of entry. A drawback associated with radioactive sources is the associated isotropic mixed neutron/gamma-ray field. This work introduces a cost-efficient test-bed for the production of 2-7 MeV neutrons based on an ^{241}Am/^{9}Be source, with the aim of lowering the barrier for precision neutron testing of detector technologies. Well-understood nuclear physics coincidence and time-of-flight measurement techniques are applied to unfold the mixed neutron/gamma-ray field and unambiguously identify the energies of the neutrons on an event-by-event basis.

List of Publications and Author's Contribution:

This thesis is based on the work presented in the following publications and manuscripts. The papers are referenced in the text using the indicated labels.

PAPER I: **Tagging fast neutrons from an ^{241}Am/^{9}Be source**

App. Rad. and Isot. **98** (2015) 74-79.

J. Scherzinger, J.R.M. Annand, G. Davatz and K.G. Fissum, U. Gendotti, R. Hall-Wilton, A. Rosborg, E. Håkansson, R. Jebali, K. Kanaki, M. Lundin, B. Nilsson, and H. Svensson

I planned, prepared and conducted the experiment. I performed the data analysis and assisted with the writing of the article.

PAPER II: **A First Comparison of the responses of a ^{4}He-based fast-neutron detector and a NE-213 liquid-scintillator reference detector**

Manuscript submitted to Nucl. Inst. and Meth. A

Preprint available at arXiv:1502.03931 [physics.ins-det]

R. Jebali, J. Scherzinger, J.R.M. Annand, R. Chandra, G. Davatz, K.G. Fissum, H. Friederich, U. Gendotti, R. Hall-Wilton, E. Håkansson, K. Kanaki, M. Lundin, D. Murer, B. Nilsson, and H. Svensson

I helped to plan, prepare and conduct the experiment. I assisted with the data analysis and contributed to the discussion presented in the manuscript.

PAPER III: **An in-depth characterization of a NE-213 reference detector with a tagged-neutron source**

Manuscript in preparation.

J. Scherzinger, K.G. Fissum, J.R.M. Annand, R. Hall-Wilton, A. Hansson, E. Håkansson, R. Jebali, K. Kanaki, M. Lundin, B. Nilsson, H. Sevensson

I planned, prepared and conducted the experiment. I performed the data analysis and wrote the article.

Other Publications to Date not Included in this Thesis:

1. **Detectors for the European Spallation Source**

   IEEE NSS/MIC (2012) *4283-4289*.

   R. Hall-Wilton, C. Höglund, M. Imam, K. Kanaki, A. Khaplanov, O. Kirstein, T. Kittelmann, B. Nilsson, and J. Scherzinger

2. **ESS Technical Design Report**

   April 23, 2013

   ESS-doc-274

   http://eval.esss.lu.se/cgi-bin/public/DocDB/ddShowDocument?docid=274

   ISBN 978-91-980173-2-8

   S. Peggs *et al.*

3. **Neutron Position Sensitive Detectors for the ESS**

   PoS (Vertex2014) *029*.

   O. Kirstein, R. Hall-Wilton, I. Stefanescu, M. Etxegarai, M. Anastasopoulos, K.G. Fissum, A. Gulyachkina, C. Höglund, M. Imam, K. Kanaki, A. Khaplanov, T. Kittelmann, Scott K., B. Nilsson, L. Ortega, D. Pfeiffer, F. Piscitelli, J. Freita Ramos, L. Robinson, and J. Scherzinger

4. **Overcoming High Energy Backgrounds at Pulsed Spallation Sources**

   Accepted by Journal of Neutron Research.

   N. Cherkashyna, R. Hall-Wilton, D.D. DiJulio, A. Khaplanov, D. Pfeiffer, J. Scherzinger, C.P. Cooper-Jensen, K.G. Fissum, S. Ansell, E.B. Iverson, G. Ehlers, F.X. Gallmeier, T. Panzner, E. Rantsiou, K. Kanaki, U. Filges, T. Kittelmann, M. Extegarai, V. Santoro, O. Kirstein, and P.M. Bentley

5. **Characterization of the radiation background at the Spallation Neutron Source**

   Manuscript in preparation.

   D. D. DiJulio, N. Cherkashyna, A. Khaplanov, D. Pfeiffer, J. Scherzinger, D. E. Hornbach, R. J. Newby, C. P. Cooper-Jensen, K. G. Fissum, E. B. Iverson, G. Ehlers, F. X. Gallmeier, K. Kanaki, R. J. Hall-Wilton, and P. M. Bentley

Contributions to Workshops and Conferences

Talks

1. **DNPLU – MAX IV –ESS Three-Party Detector Lab**
   In-Kind and Collaborative Detector Meeting, Lund, Sweden, 2013
2. **Scintillators – Neutron Detection from MeV to ….(meV)**
   SFAIR and Swedish Nuclear Physicists Meeting, Stockholm, Schweden, 2013
3. **A Neutron Source Facility for Energy Dependent Detector Characterization**
   Position Sensitive Neutron Detector Workshop, Jülich, Germany, 2014

Posters

1. **Novel Scintillator Materials for Neutron Detection**
   IKON 3, Lund, Sweden, 2012
2. **Characterization of a Liquid Scintillator Detector**
   IKON 3, Lund, Sweden, 2012
3. **Characterization of a Liquid Scintillator Detector with an Americium-Beryllium source**
   IKON 4, Lund, Sweden, 2013
4. **A broad-band neutron source facility for detector characterization**
   IEEE NSS/MIC, Seattle, USA, 2014

Contents

List of Figures

List of Tables

Abbreviations

ADC	Analog-to-Digital Converter
Am/Be	Americium-Beryllium
CAD	Computer-Aided Design
CAMAC	Computer Automated Measurement And Control
DAQ	Data Acquisition
DRS	Domino-Ring Sampler
ESS	European Spallation Source
FOM	Figure-of-Merit
FPGA	Field-Programmable Gate Array
FWHM	Full-Width at Half-Maximum
GSPS	Giga-Samples Per Second
L	Light Yield
LG	Long Gate
MSPS	Mega-Samples Per Second
NDT	Neutron Diagnostic Tool
NIM	Nuclear Instrumentation Module
PMMA	Poly-Methyl-Methacrylate
PMT	Photomultiplier Tube
PH	Pulse Height
PHD	Pulse-Height Discrimination
PS	Pulse Shape
PSD	Pulse-Shape Discrimination
PTFE	Polytetrafluoroethylene
QDC	Charge-to-Digital Converter
SG	Short Gate
TDC	Time-to-Digital Converter
TOF	Time-of-Flight
VME	Versa Module Europa
YAP	Yrtium Aluminum Pervokite

1 Introduction

Both thermal and fast neutrons are important probes of matter [1–7] and are used in a wide variety of fields from fundamental physics and material science to geological studies and homeland-security applications. One of the most common detector materials for neutrons of all energies is ^{3}He. In the last decade, the stockpile of this scarce resource was depleted and its price has become too great for large-scale detector applications [8–10]. This "^{3}He crisis" [8–12] has triggered a renewed interest in the neutron-scattering community into new detector technologies to replace existing technologies used for large-area detectors [13, 14]. Many of these replacement technologies are still in their infancy [15], while others have been successfully tested and are approaching maturity [16] and still others have been in common use for years [17].

New technologies need to be tested in well-defined laboratory environments. Essential to these are sources of neutrons for controlled irradiation – accelerators, nuclear reactors and radioactive sources. Neutrons produced in nuclear reactors and at accelerators have a very high cost per neutron and a high cost of entry. In contrast, radioactive sources produce neutrons at a substantially lower cost per neutron. A drawback associated with radioactive sources is the isotropic mixed neutron/gamma-ray fields. This work describes the development of a cost-efficient precision test-bed for the production of 2-7 MeV neutrons which is based on an ^{241}Am/^{9}Be source (hereafter referred to as Am/Be) [18]. At this test-bed, well-understood shielding, coincidence, and time-of-flight measurement techniques are employed to attenuate and subsequently unfold the mixed decay-product radiation field[1] provided by the Am/Be, resulting in a polychromatic energy-tagged neutron beam.

This thesis is divided in three parts. A short introduction to the measurement apparatus, including both the setup and the equipment, is given in Chapter 2. Chapter 3 is used to present detector characterization using a standard neutron irradiation and one using "tagged" neutrons. Chapter 4 is used to summarize the work and present an outlook for the development of a dedicated test facility. The three papers upon which this Licentiate Thesis is based are attached in the Appendix.

[1] The concepts and procedures discuseed in this thesis will work equally well for any Be-based radioactive neutron source.

2 Apparatus

An overview of the equipment and the experimental setup is given. Shielding, source, detectors, electronics and data acquisition are described.

2.1 Neutron Source

At the heart of the facility is a nominal 18.5 GBq Am/Be radioactive source [18] which emits $(1.106 \pm 0.015) \times 10^6$ neutrons per second nearly isotropically [18]. Both the gamma-ray and neutron dose rates at a distance of 1 m from the unshielded source were measured using a Thermo Scientific Corporation FHT 752 dosimetric neutron/gamma-ray detector [19]. They were determined to be 11 μSv/h each. The source is a mixture of americium oxide ($^{241}AmO_2$) and beryllium metal (^{9}Be) encapsulated in a X.3 capsule. X.3 capsules (see Fig. 2.1) are tig-welded, double-layered, stainless-steel cylinders 31 mm in height $\times$ 22.4 mm in diameter. ^{241}Am has a half-life of 432.2 years and decays via 5 discrete α-emissions (average energy of 5.5 MeV) to ^{237}Np. The dominant energy of the gamma-rays from the decays of the intermediate excited states of ^{237}Np is $\sim$60 keV. A 3 mm thick Pb sheet was used to suppress $\sim$80% of these 60 keV gamma-rays as the half-value layer for 60 keV gamma-rays for Pb is 0.12 mm. The daughter ^{237}Np has a half-life of over 2 million years. ^{9}Be is stable. Fast neutrons are emitted when α-particles interact with ^{9}Be, producing ^{12}C and a free-neutron.

The precise free-neutron distribution, particularly the energies and relative intensities of the peaks forming the sub-structure in the spectrum, varies depending upon the properties of the Am/Be source containment capsule and the size of the $^{241}AmO_2$ and Be particles in the powders employed [20]. That said, some general statements about the fast-neutron distribution can be made. Am/Be sources produce free neutrons having a maximum energy of about 11 MeV. Approximately $\sim$25% of the neutrons emitted have an energy of less than $\sim$1 MeV with a mean energy of $\sim$400 keV [18]. The average fast-neutron energy is $\sim$4.5 MeV. The kinematics and the reaction cross section for the ^{9}Be(α,n) interaction determine the state of the recoiling ^{12}C nucleus produced in the reaction. Independent calculations suggest that the relative populations of the ground, the first-excited and the second-excited states for the recoiling ^{12}C nucleus are $\sim$35%, $\sim$55% and $\sim$15% respectively [21–23]. ^{12}C nuclei excited to the first-excited state will promptly decay to the ground state by the isotropic emission of 4.44 MeV gamma-rays. The resulting gamma-ray to neutron ratio R has

been measured to be ∼0.58 [24, 25], in good agreement with theoretical calculations. It follows that between 55% and 60% of the neutrons emitted by an Am/Be source are accompanied by a prompt, time-correlated 4.44 MeV gamma-ray. This property may be used to measure the elapsed time between the detection of the 4.44 MeV gamma-ray and the fast neutron, yielding the neutron time-of-flight and thus kinetic energy. This procedure is known as "tagging". The available tagged-neutron energies are thus necessarily restrict to a maximum value of less than 7 MeV as 4.44 MeV of the reaction Q-value are lost to the de-excitation gamma-ray.

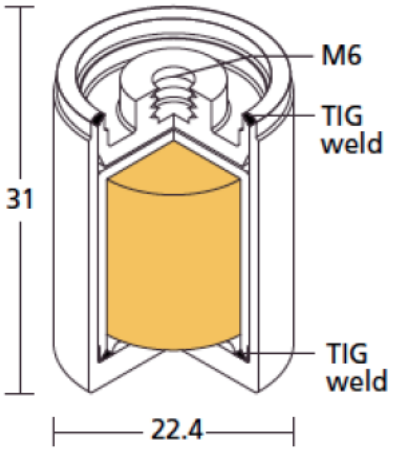

Figure 2.1: A schematic drawing of the Am/Be source [18]. The dimensions are given in mm. The yellow shaded volume at the central core of the capsule corresponds to the Am/Be mixture.

2.2 Source Tank and Shielding

A water-filled tank (see Fig. 2.2 (d)) is used to define beams of neutron and gamma-rays coming from the source. The design of the water tank was developed with both functionality and safety in mind. First tests of the neutron-tagging technique were performed with a temporary assembly made from concrete blocks, borated paraffin boxes and water jugs (see Fig. 2.2 (a)). The paraffin boxes were judged to be too dangerous for permanent shielding due to the associated fire hazard. It was therefore decided to employ water for the bulk shielding. A FLUKA [27] simulation[2] was used to determine the minimum thickness of pure-water shielding which could reduce the total dose rate at the exterior surface of the source tank to less than 0.5 μSv/h. If the source is located in the designated "park" position, the construction fulfills this

[2]The simulation was written as part of a radiological survey of the above mentioned Am/Be source by Magnus Lundin of the Radiation Safety Group at the MAX IV Laboratory [28].

(a)

(b)

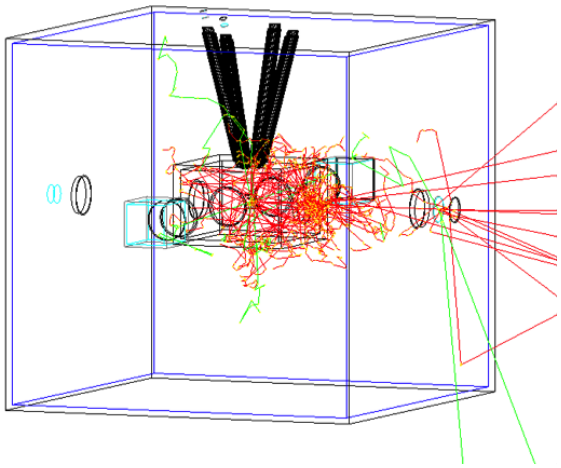

(c)

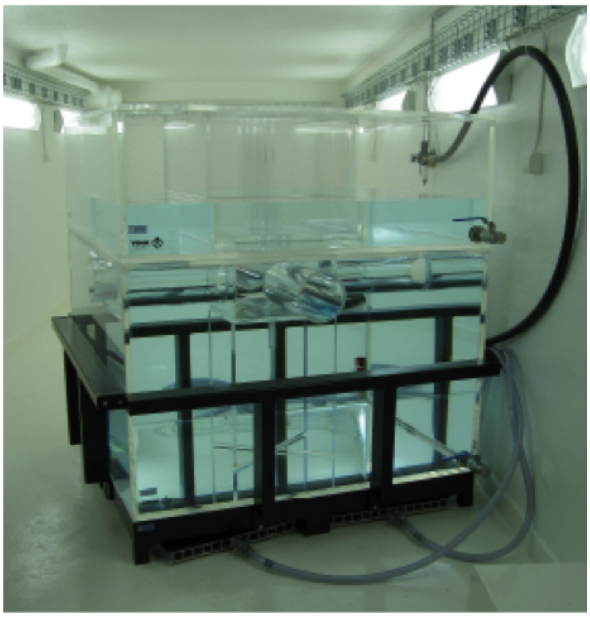

(d)

Figure 2.2: The development of the shielding design. The temporary wax-box and water jug shielding is shown in pad (a). An early CAD image of the source tank is shown in pad (b). The visualization of a Geant 4 simulation [26] of the shielding assembly is shown in pad (c). The assembled, partially filled tank is shown in pad (d). Note the airpad frame which allows for effortless repositioning.

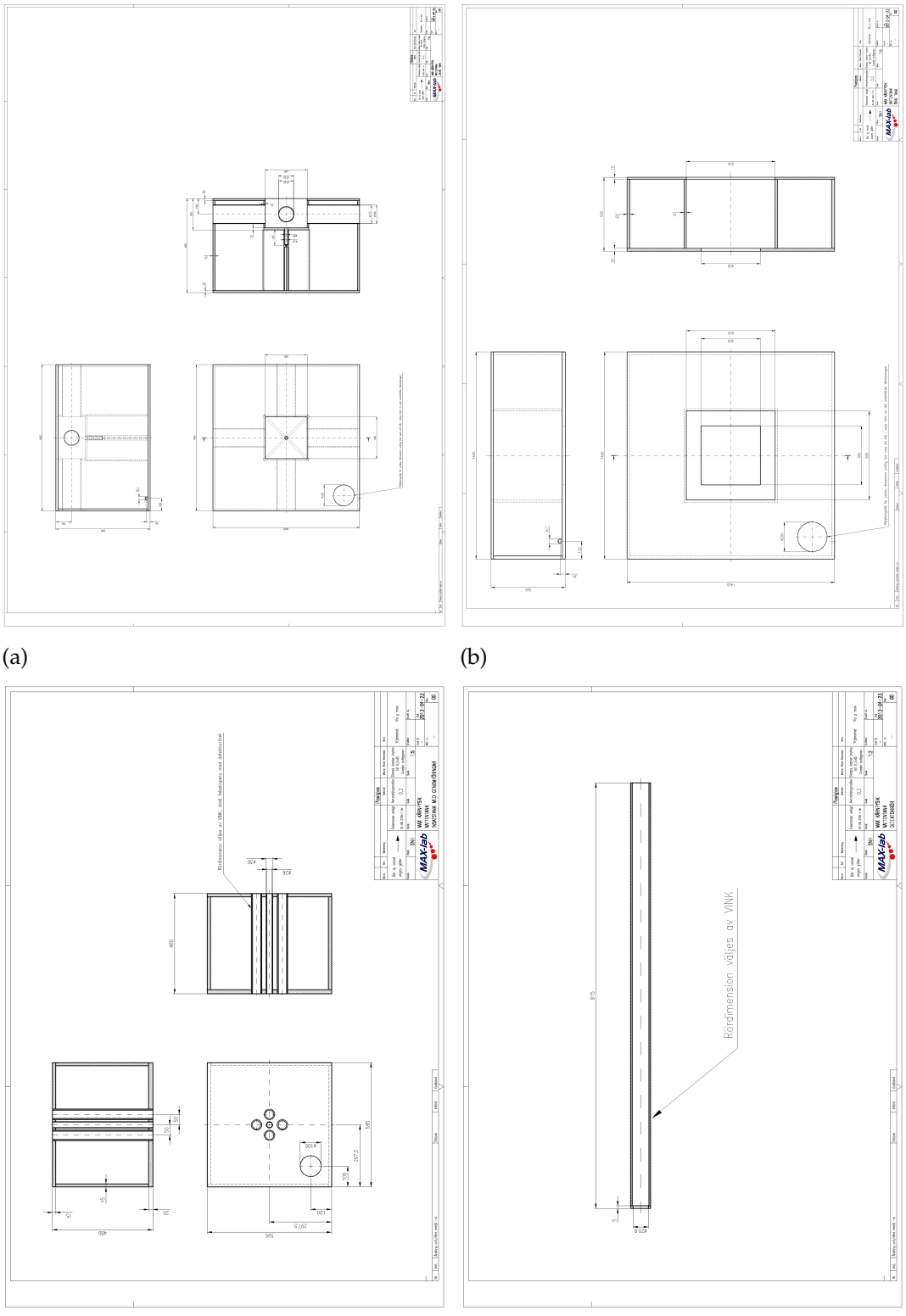

(a) (b)

(c) (d)

Figure 2.3: CAD drawings of the three modules of the source tank. The lower tank is shown in pad (a), the upper tank is shown in pad (b), the inner tank is shown in pad (c), and a PMMA sleeve used to position a YAP detector (see Section 2.3) is shown in pad (d).

requirement. The tank is made from poly-methyl-methacrylate (PMMA), also known as plexiglass and lucite, and was produced by VINK in Malmö [29]. The tank has outer dimensions of 1400 mm $\times$ 1400 mm $\times$ 1400 mm. A three piece modular design was chosen to increase accessibility to the inner chamber in the lower tank (see Fig. 2.3 (a)). The inner chamber (400 mm $\times$ 400 mm $\times$ 280 mm) houses the neutron source and up to 4 YAP detectors (see Section 2.3). The open top of this chamber is normally covered by both the upper tank (see Fig. 2.3 (b)) and the inner tank (see Fig. 2.3 (c)). PMMA sleeves (see Fig. 2.3 (d)) are used to set the YAP detectors in well-defined positions. These sleeves are inserted through designated openings in the inner-tank module (see Fig. 2.3 (c)) 30 mm in diameter and 480 mm in length. A fifth slightly smaller vertical penetration (26 mm in diameter) for the source is located in the geometrical center of the tank. The tank is filled with ~2650 liters of ultra pure, de-ionized water. Four beamports 172 mm (diameter) and 500 mm (length) allow for simultaneous irradiations of four independent experiments. CAD drawings of the modules described are shown in Fig. 2.3.

2.3 The YAP Scintillator Detector

Figure 2.4: Photograph of a YAP detector.

To detect the 4.44 MeV gamma-rays, cerium activated ytrium aluminum pervoskite (YAP:Ce^{3+}) single-crystal detectors are used. These fast (~5 ns risetime) scintillator detectors were supplied by Scionix [30]. The detectors are composed of 1 inch (diameter) $\times$ 1 inch (height) single-crystal cylinders which are coupled to a 1 inch R1924 Hamamatsu photomultiplier tube (PMT) [31]. The PMTs are operated at about -800 V. The energy resolution of the detectors was determined to be ~10% at 662 keV using ^{137}Cs. The YAP detectors are not used for spectroscopy but rather as trigger detectors. YAP is an excellent choice for a gamma-ray detector operated near an intense neutron source. The material is radiation hard and is quite (but not completely) insensitive to neutrons of all energies.

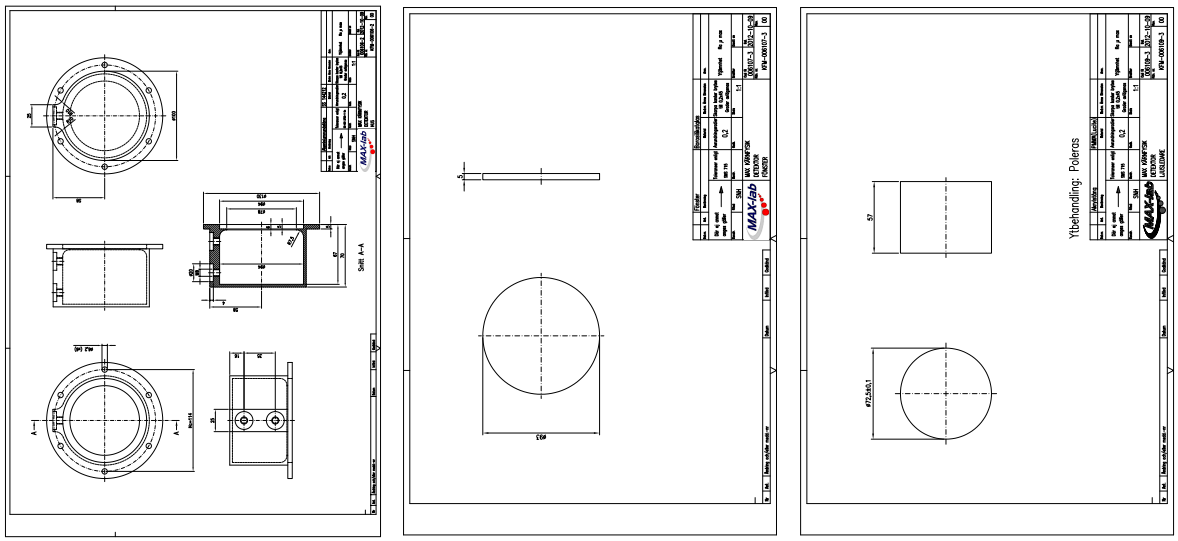

(a) (b) (c)

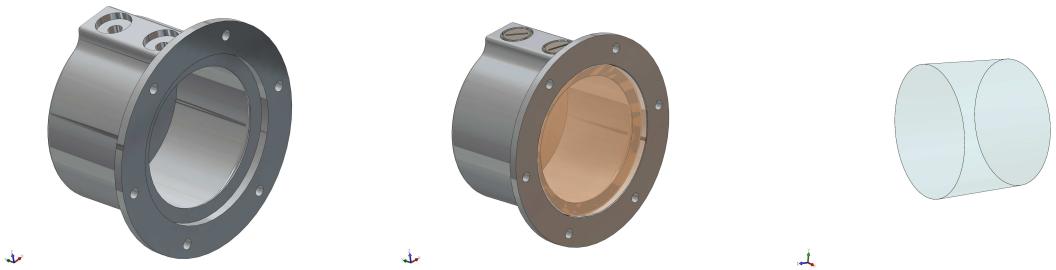

(d) (e) (f)

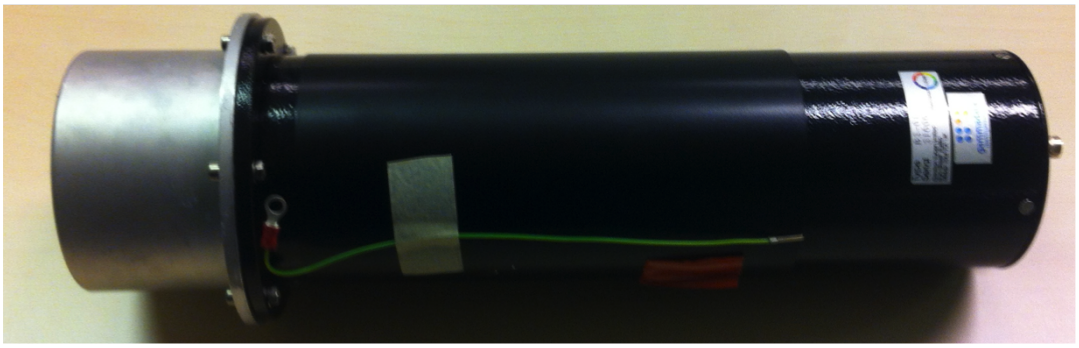

(g)

Figure 2.5: The top panel shows the CAD drawings of the NE-213 liquid scintillator detector parts; the aluminum cell in pad (a), the glass window in pad (b) and the light guide in pad (c). The middle panel shows the corresponding CAD images. The bottom shows a photograph of the assembled detector. The black tube attached to the detector cell is a magnetically shielded 3 inch ET Enterprises 9821KB PMT assembly.

2.4 NE-213 Liquid Scintillator Detector

The assembled fast-neutron detector used for the measurements put forth in this thesis and its components are shown in Fig. 2.5. The NE-213 detector is sensitive to both gamma-rays and fast neutrons. The detector consisted of a 3 mm thick aluminum cell with a 94 mm inner diameter and a 62 mm inner depth (see Figs. 2.5 (a) and (d)) filled with $\sim$430 ml of NE-213 [32]. NE-213 is a commonly used liquid organic scintillator for fast neutron detection based on xylene, an aromatic molecule of the formula $C_6H_4(CH_3)_2$. The scintillator emits light at 425 nm and has a bulk light attenuation length of $\sim$3 m. The cell was sealed with a 5 mm thick borosilicate glass window [33] (see Figs. 2.5 (b) and (e)) using Araldite 2000+ [34] glue which is highly resistant to both temperature and chemicals. Two penetrations, sealed by M8 threaded aluminum screws with 20 mm diameter heads and 14 mm diameter Viton O-rings [35], were used to fill the detector. The inner walls of the detector were painted with the reflective paint EJ-520 [36]. This paint is able to withstand the highly aggressive solvents in the scintillator. The scintillator was flushed with nitrogen before it was transferred to the detector cell. In addition, a nitrogen-transfer system was used to fill the cell. This nitrogen flushing reduced oxygen residue in the scintillator. The filled cell was coupled to a 72.5 mm (diameter) $\times$ 34 mm (length) PMMA lightguide [37] (see Figs. 2.5 (c) and (f)). Acrylic PMMA transmits light down to wavelengths of 300 nm [38]. The lightguide wall was painted with water-soluble EJ-510 [39] reflective paint. The lightguide was pressure-coupled to a spring-loaded, magnetically shielded 3 inch ET Enterprises 9821KB PMT assembly [40] operated at about -2000 V. To ensure the reproducibility of the behavior of the detector over an extended period of time, optical grease was not used in the assembly.

2.5 The ^{4}He-based Neutron Diagnostic Tool

The neutron diagnostic tool (NDT) from Arktis Radiation Detectors [41] (Arktis) used in these measurements is shown in Fig. 2.6. The pressure vessel, a stainless-steel tube with an outer diameter of 5.08 cm and an active length of 19.5 cm, was sealed on both ends with optical windows. ^{4}He was filled into the active detector volume to a pressure of 120 bar. The interior surface of the stainless-steel cylinder was coated with a PTFE-based diffuse reflector [42] which was itself coated with an organic phosphor that converted the wavelength of the scintillation light from 80 nm to 430 nm. Signal loss in the detector was almost exclusively due to multiple reflections inside the detector. Light losses due to re-absorption in the detector medium were negligible, since ^{4}He is essentially transparent to its own scintillation light [43]. The scintillation pulses were read out via both optical windows by dry-fitted Hamamatsu R580 [44] PMTs.

2.6 Experimental Setup

Two different experimental setups were used in this work. In PAPER I, the method of neutron-"tagging" is explained. In PAPER II, detectors were simply irradiated. In PAPER III, the neutron-tagging technique was employed and YAP detectors were used to pick off the 4.44 MeV gamma-rays corresponding to fast-neutron production.

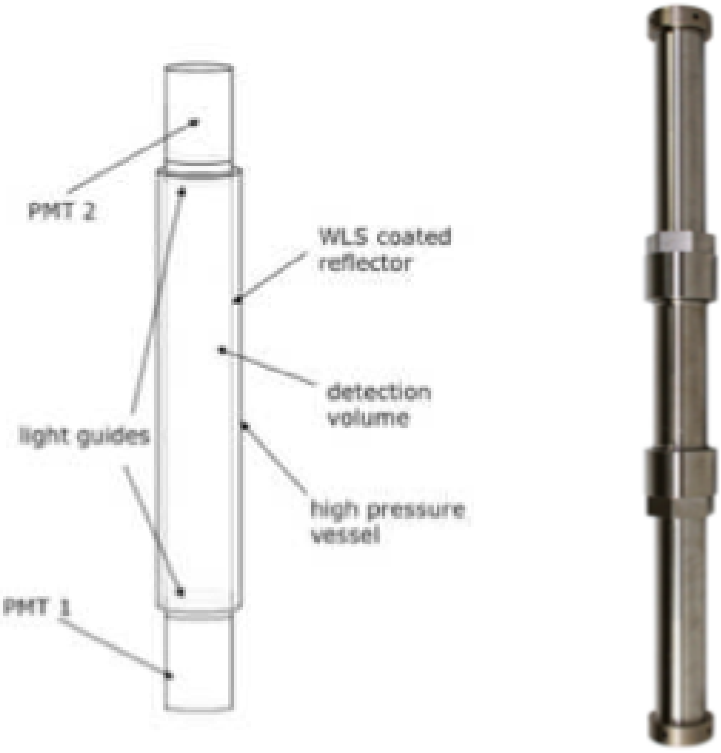

(a) (b)

Figure 2.6: Schematic (a) and photograph (b) of the pressurized ^{4}He noble-gas fast-neutron detector. The outer diameter was 5.08 cm and the active length was 19.5 cm.

2.6.1 Free Irradiation

When detectors were irradiated freely, shielding was employed to reduce the dose to personnel. Figure 2.7 shows a schematic drawing of the first use of this mode with preliminary shielding provided by borated-wax boxes. The NE-213 reference cell and the Arktis NDT were irradiated simultaneously.

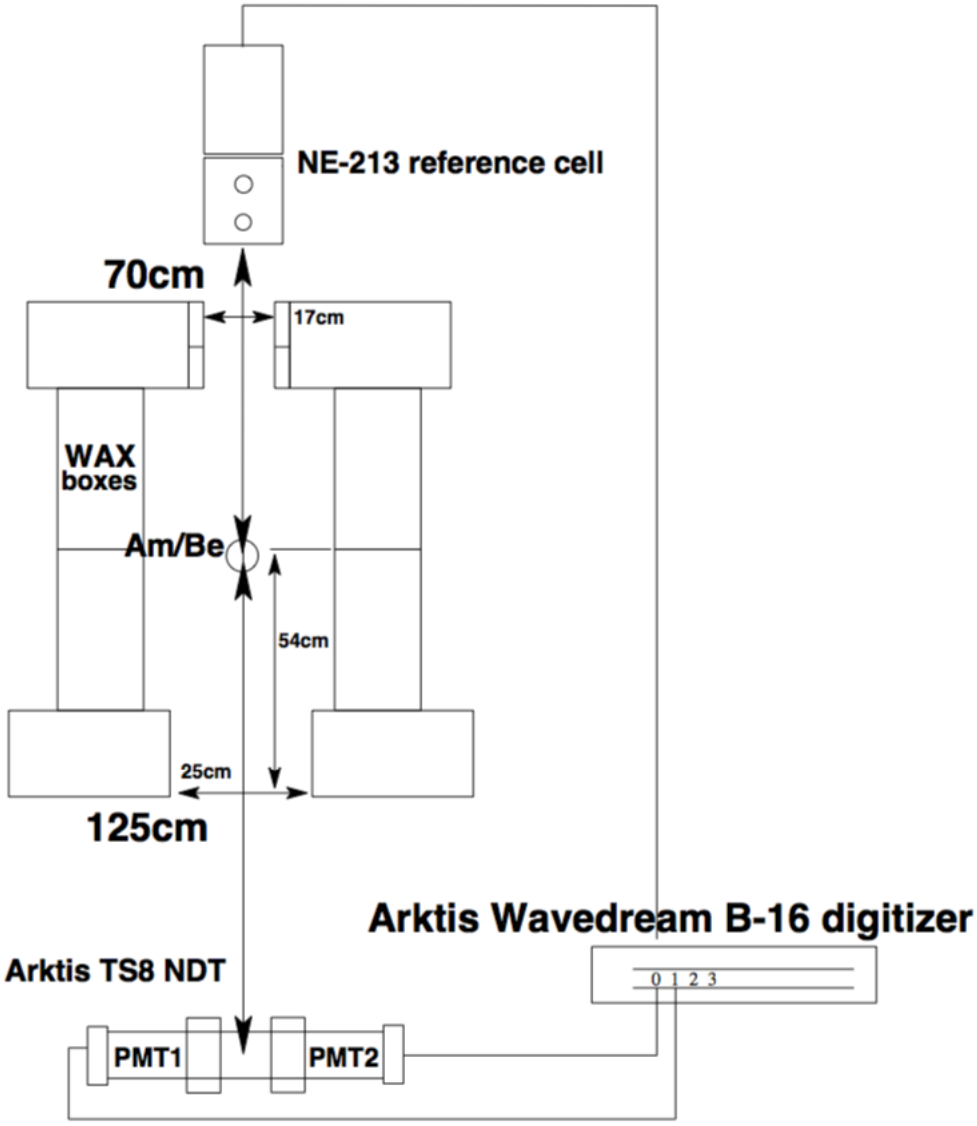

Figure 2.7: A simplified overview of the experimental setup for free irradiation (not to scale). The Am/Be source, wax shielding, NE-213 reference detector and NDT are shown.

2.6.2 Tagging Neutrons

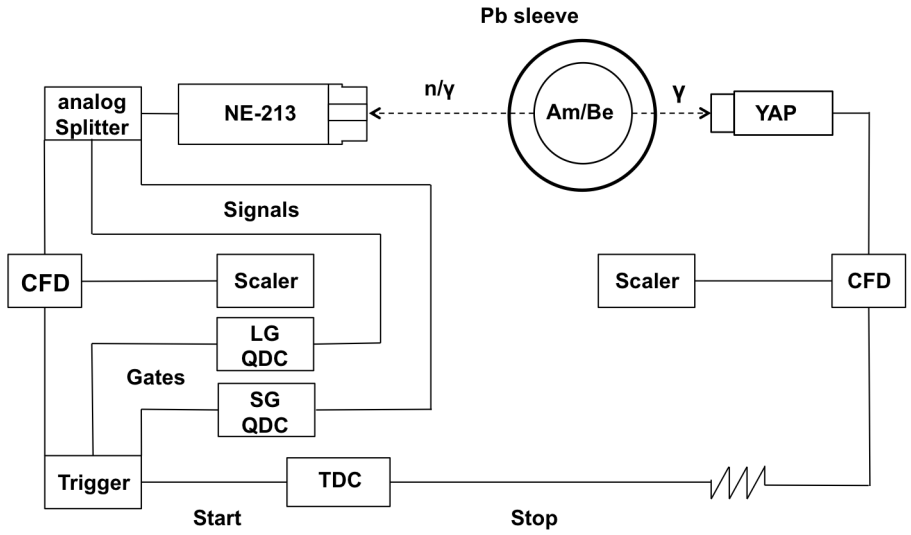

Figure 2.8: A simplified overview of the experimental setup (not to scale). The Am/Be source, the Pb sleeve, a single YAP detector, and the NE-213 detector are all shown together with a block electronics diagram.

A block diagram of the tagging configuration is shown in Fig. 2.8. The Am/Be source was placed so that its cylindrical-symmetry axis corresponded to the vertical direction in the lab at the center of a 3 mm thick cylindrical Pb sleeve (with the same orientation) to attenuate the associated 60 keV gamma-rays. A YAP detector was placed with its crystal approximately 5 cm from the Am/Be source at source height. The crystal orientation was such that its cylindrical symmetry axis also corresponded to the vertical direction in the lab. This detector triggered overwhelmingly on the 4.44 MeV gamma-rays radiating from the source which came from the decay of the first excited state of ^{12}C. The NE-213 cell was placed at 0.68 m, the flight path, from the Am/Be source at source height and was free-running. It triggered on both 4.44 MeV gamma-rays and fast neutrons coming from the source, as well as cosmic rays and room background.

2.7 Data Acquisition and Electronics

Two different data-acquisition (DAQ) systems were used for this work. For the initial development of the source facility (PAPER I) and the in-depth characterization of the NE-213 fast neutron reference cell (PAPER III), a customized version of the DAQ developed by the Photonuclear Group at The Max IV Laboratory [28] was used. For

the comparison study between NE-213 and the NDT (PAPER II), a table-top digitizer based on the DRS4 chip [45] developed by Arktis Radiation Detectors was used.

2.7.1 The MAX IV Laboratory System

Signals were recorded on an event-by-event basis for offline analysis using a LINUX PC DAQ system. The DAQ uses the C++ based data-analysis framework ROOT [46] to provide online data monitoring and data storage. The analog signals from the NE-213 detector and the YAP trigger detectors were passed to LRS 2249A and LRS 2249W CAMAC charge-to-digital converters (QDCs) and PS 715 NIM constant-fraction (timing) discriminators. The logic signals from the discriminators were passed to LRS 4434 scalers and LRS 2228A CAMAC time-to-digital converters (TDCs). The VME and CAMAC crates were connected to the PC by a SBS 616 PCI-VME bus adapter and a CES 8210 CAMAC branch driver.

In time-of-flight (TOF) mode, signals from the NE-213 detector were used to trigger the DAQ. The NE-213 detector QDCs included a 60 ns short-gated (SG) QDC (LRS 2249A) and a 500 ns long-gated (LG) QDC (LRS 2249W), both of which opened 25 ns before the analog pulse arrived. The NE-213 detector also provided the start trigger for the TOF TDC. The YAP detector provided the stop trigger for the TOF TDC. To reduce deadtime, events seen only by the YAPs were rejected by triggering the DAQ system exclusively on the NE-213 detector.

2.7.2 WaveDREAM Digitizer

A WaveDREAM-B16 digitizer was supplied by Arktis Radiation Detectors. The digtizer supplies both excellent resolution at 10 bits and excellent timing resolution at 1 gigasample per second (GSPS). The pulses were not processed before digitization. The NDT and NE-213 detector signals were fed directly to 3 of the 16 channels of the digitizer. The digitized signals were read out via a Gigabit ethernet connection and stored for offline analysis. Data were collected when a 120 megasample per second (MSPS) signal that was continuously read out and processed by a field-programmable gate array (FPGA) met the user-defined trigger conditions. When the system was triggered, the FPGA read out the 3.5 μs long, stored waveform at 1 GSPS from the DRS 4 chip[3] [45]. In the case of the NE-213 detector, a trigger occurred if the analog PMT signal met a threshold condition of at least 30 scintillation photons above the ambient baseline. The NDT triggered if both PMTs detected at least 35 scintillation photons above the ambient baseline. An NDT event was considered valid if both NDT PMTs signals arrived within 32 ns of each other. The offline analysis of the data was greatly facilitated by the digitization of the waveform. Both NDT PMTs can be synchronized to better than 1 ns and the detector thresholds and integration gates can be adjusted

[3]The DRS 4 is a switched capacitor array developed by the Paul Scherrer Institute.

offline, which is a clear advantage over standard discriminators and analog-to-digital converters.

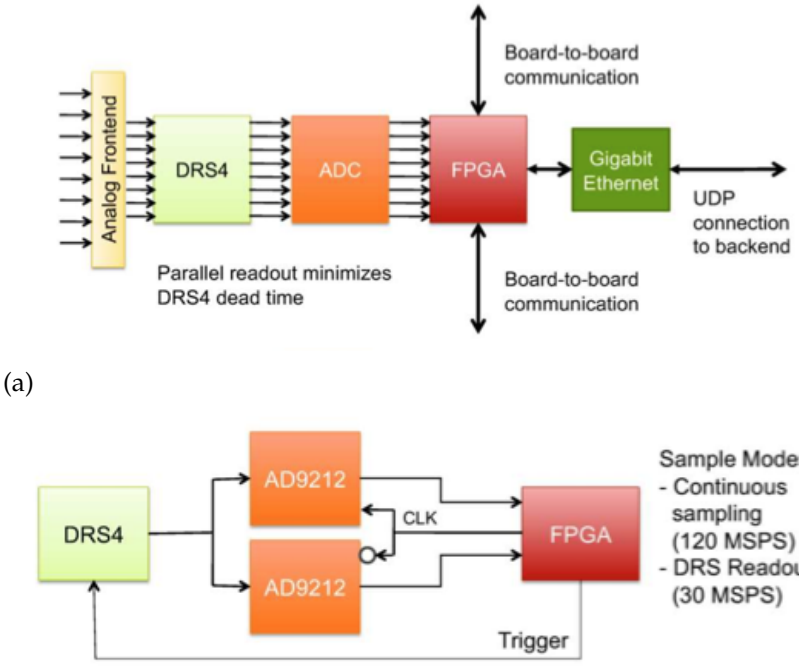

(a)

(b)

Figure 2.9: The Arktis Radiation Detectors WaveDREAM digitizer. Pad (a) presents an overview of the readout electronics. Signals were stored in the DRS 4 switched-capacitor array. Stored pulses were read out if they met the user-defined trigger conditions. Pad (b) gives a schematic representation of the software trigger. If the continuously read 120 MSPS signal met the trigger conditions, the DRS 4 chip was read out at 1 GSPS by the FPGA. [47]

3 Data Analysis

This chapter presents a general overview of the data analysis and the detector-characterization methods which were used. The detector-characterization method varied depending on whether a simple irradiation or tagged neutrons were employed.

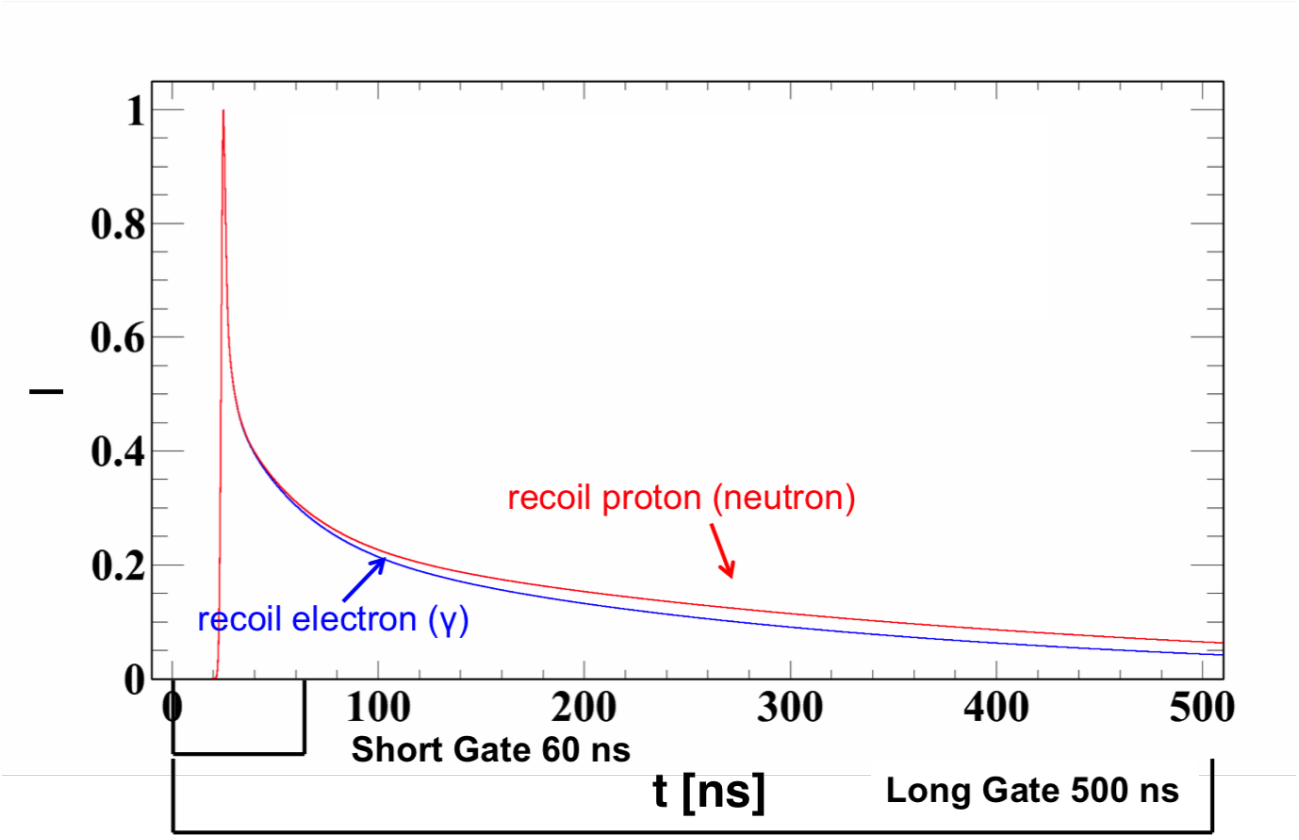

Figure 3.1: Schematic representation of the light pulse for neutron-induced recoiling protons (in red) and for gamma-ray-induced recoiling electrons (in blue) in liquid scinillators such as NE-213. Also shown are the short and the long QDC gates employed.

3.1 Free Irradiation

Free irradiation is the simplest way to use the test-bed for detector characterization. Scintillator detectors can be investigated directly for their intrinsic neutron/gamma-ray discrimination capabilities.

3.1.1 Pulse Shape

The mixed neutron/gamma-ray field from the Am/Be source was used to establish pulse-shape discrimination (PSD) between gamma-ray-induced recoiling electrons and neutron-induced recoiling protons and to measure light yield dependent figures-of-merit (FOM) (see blow). In measurements performed with the MAX IV Laboratory DAQ, the analog detector signal was split and the current of each was integrated independently in the SG QDC and the LG QDC with 60 ns and 500 ns integration gates respectively (see Fig. 2.8). Signal splitting was not necessary for data collected with the WaveDREAM-B16 digitizer. Integration gates were applied to the digitized pulses offline.

The different shapes of the light pulses from gamma-ray-induced recoiling electrons and from neutron-induced recoiling protons (NE-213) (see Fig. 3.1) or recoiling alpha-particles (^{4}He) was measured using the so-called "Tail-to-Total" Charge Comparison Method [48–50]. The pulse-shape function (PS) was defined by the difference of the charges measured by the LG QDC and the SG QDC normalized to the LG QDC charge

$$PS = \frac{LG\ QDC - SG\ QDC}{LG\ QDC}. \tag{3.1}$$

3.1.2 Pulse-Shape Discrimination

Most scintillator detectors have a linear correlation between the energy deposited by an electron and the numbers of scintillation photons emitted. The signal produced by an analog-to-digital converter (ADC), such as the QDCs in the MAX IV Laboratory DAQ and the Arktis Radiation Detectors digitizer, is proportional to the number of scintillation photons detected by a PMT. It is convenient to express this signal in units of electron-equivalent energy MeV_{ee}, since ADC channels are easily calibrated using standard gamma-ray calibration sources such as ^{137}Cs, ^{22}Na and ^{60}Co and the Knox Method [51]. In the following, ADC signals will be referred to as light yields L.

Figure 3.2 shows a contour plot of PS plotted against the light yield L for the NE-213 detector measured with the MAX IV Laboratory DAQ. The excellent discrimination between neutron and gamma-ray events is apparent for $L > 0.5\ MeV_{ee}$. A small overlap exists between the two distributions below this threshold in the vicinity of PS = 0.2.

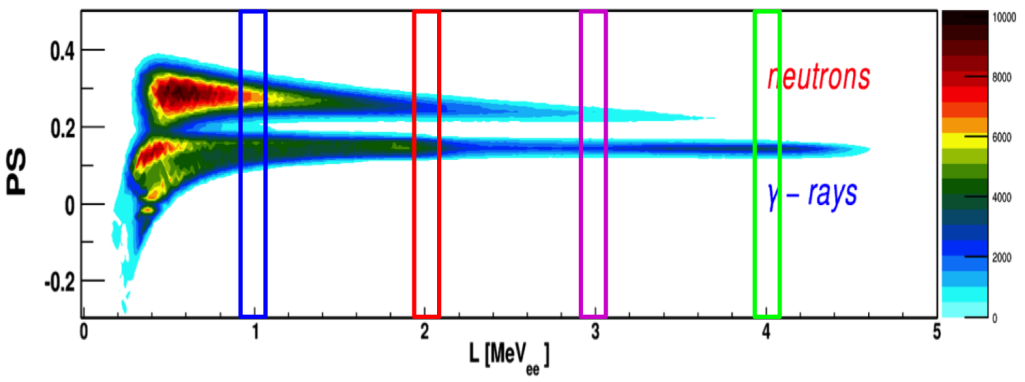

Figure 3.2: Contour plot of PS versus light yield L in MeV_{ee} for the NE-213 detector. The data were collected with the MAX IV Laboratory DAQ.

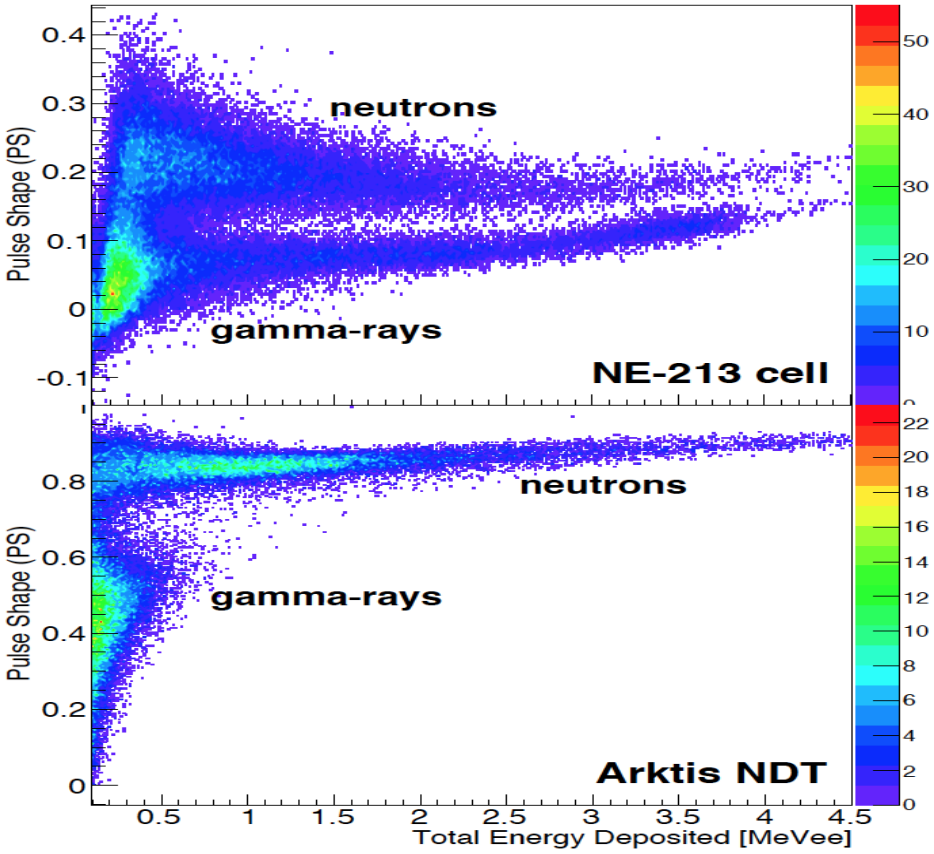

Figure 3.3: Scatter plots of PS versus the light yield L for both the NE-213 detector and the NDT measured with the Arktis Radiation Detectors digitzer.

In Figure 3.3, scatter plots of the PS versus L are shown for both the NE-213 de-

tector (top panel) and the NDT (bottom panel) measured with the WaveDREAM digitizer. The difference in the shape of the NE-213 response shown in Fig. 3.2 and Fig. 3.3 can be explained by the different lengths of the integration gates. The discrimination between neutron and gamma-ray interactions is excellent. The NDT shows even better PSD for neutrons and gamma-rays. It is excellent down to a threshold of L = 0.2 MeV_{ee}. The most striking difference between both detectors is illustrated by the gamma-ray responses. The NDT registers an energy maximum of 750 keV_{ee} regardless of the energy of the incident gamma-ray. This improves the neutron/gamma-ray discrimination of the detector and allows for discrimination of gamma-rays based on the pulse height, a clear advantage over liquid-scintillator detectors.

3.1.3 Figures-of-Merit

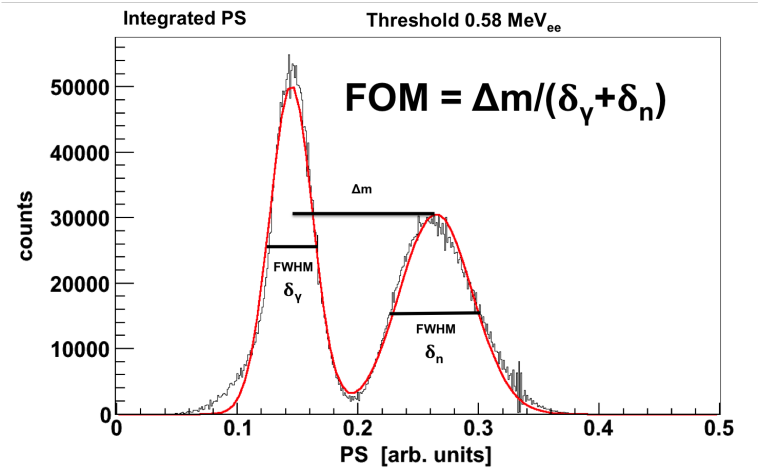

Figure 3.4: An integrated PS plot for all light yields larger than 0.58 MeV_{ee} is shown as an example of a FOM. These are data from the NE-213 detector taken with the MAX IV Laboratory DAQ.

An integrated PS spectrum (L $\geq$ 0.58 MeV_{ee}) is shown in Fig. 3.4. Two peaks are clearly visible. Events below PS = 0.2 correspond to gamma-ray induced recoiling electrons. Events above PS = 0.2 correspond to neutron-induced recoiling protons. The FHWMs of the Gaussian fits $\delta_{n,\gamma}$ and the positions of the means $m_{n,\gamma}$ are used to calculate the FOM = 1.03 of the detector for a 0.58 MeV_{ee} pulse-height threshold cut. The FOM is defined as

$$FOM = \frac{|m_n - m_\gamma|}{\delta_n + \delta_\gamma}. \tag{3.2}$$

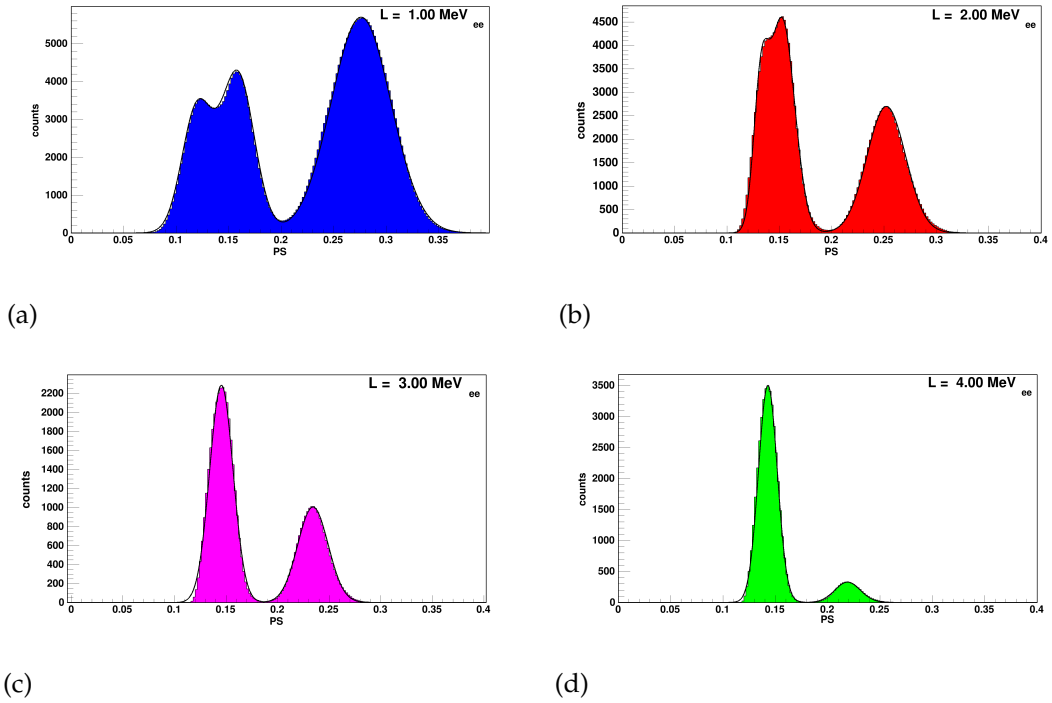

Figure 3.5: Differential PS spectra for four different pulse heights corresponding to the colored bins in Fig. 3.2. The bin width used to create these spectra was 0.1 MeV_{ee}. Gaussian fits from which FOMs are determined are shown in black.

The strength of the PSD and therefore the FOM are functions of the light yield. This is illustrated in both Fig. 3.6 and Fig. 3.5 by the increase in the gap between the neutron and the gamma-ray distributions for larger L. Differential figures-of-merit for the NE-213 detector were established by dividing the PSD plot into light yield intervals with a bin width of 0.1 MeV_{ee}. The FOMs were determined by Gaussian fits. Below 2.2 MeV_{ee}, the FOM was calculated by fitting a double Gaussian function to the gamma-ray distribution and a single Gaussian function to the neutron distribution. The double Gaussian function was then folded to a single distribution. For all other pulse heights, single Gaussian functions were fitted to both the gamma-ray and the neutron distributions. Fig. 3.5 shows PS spectra for 4 light yields. It can be observed that the FWHMs of the both the gamma-ray and the neutron distributions decrease for higher light yields. In Fig. 3.6, the integrated PS of both the NDT and the NE-213 detectors measured with the Arktis Radiation Detectors digitizer are shown for five light yield thresholds. Note that they are integrated and not differential PS spectra. The FOM of the NE-213 detector behaves comparably to the FOM determined with the MAX IV Laboratory DAQ. For thresholds below 750 keV_{ee}, the FOM achieved with the NDT is larger than the FOM achieved by the NE-213 detector. The real difference between the two detector systems can be seen for thresholds above

750 keV_{ee}. The neutron/gamma-ray discrimination is excellent and allows for both PSD and pulse-height discrimination (PHD).

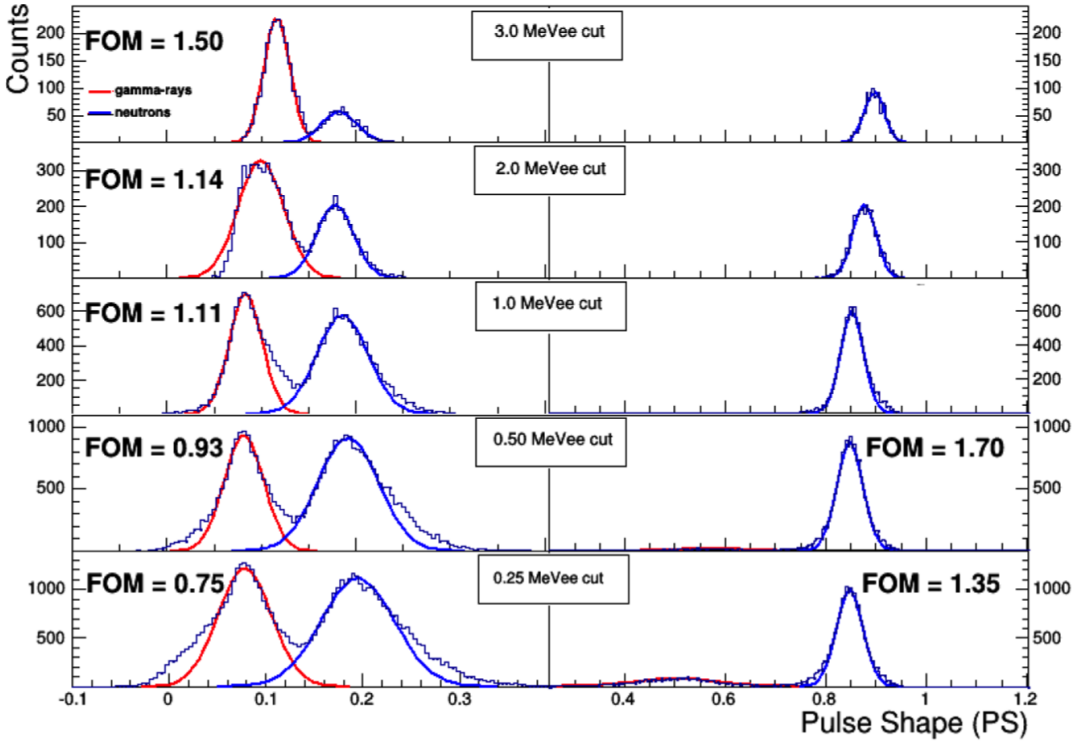

Figure 3.6: Integrated PS plots for both the NE-213 (left side) and the NDT (right side) data measured with the Arktis Radiation Detectors digitzer at 5 different threshold cuts. The achieved FOM are stated.

3.2 Tagged Neutrons for Time-of-Flight Measurements

For more advanced detector characterizations, knowledge of the incident neutron energy is important. The following gives a brief introduction to TOF spectroscopy as one example of the advantage of the neutron-tagging technique. The transformation from TOF frame-of-reference to the neutron kinetic energy frame-of-reference is described and the neutron-induced recoil-proton light yield in the NE-213 detector is determined.

3.2.1 Time-of-Flight

Figure 3.7 presents a TOF distribution for the NE-213 detector obtained with a hardware threshold of 250 keV_{ee}. The top panel, a contour plot of PS versus TOF, shows

excellent separation of both particle species in both TOF and PS. Neutrons can easily be identified. The second panel shows the neutron (shaded in red) and gamma-ray (non-shaded in blue) TOF distributions. The sharp blue peak centered at about 2 ns is known as the gamma-flash. This peak corresponds to a pair of prompt, time-correlated gamma-rays produced in the source which triggered both the NE-213 detector and the YAP detector.

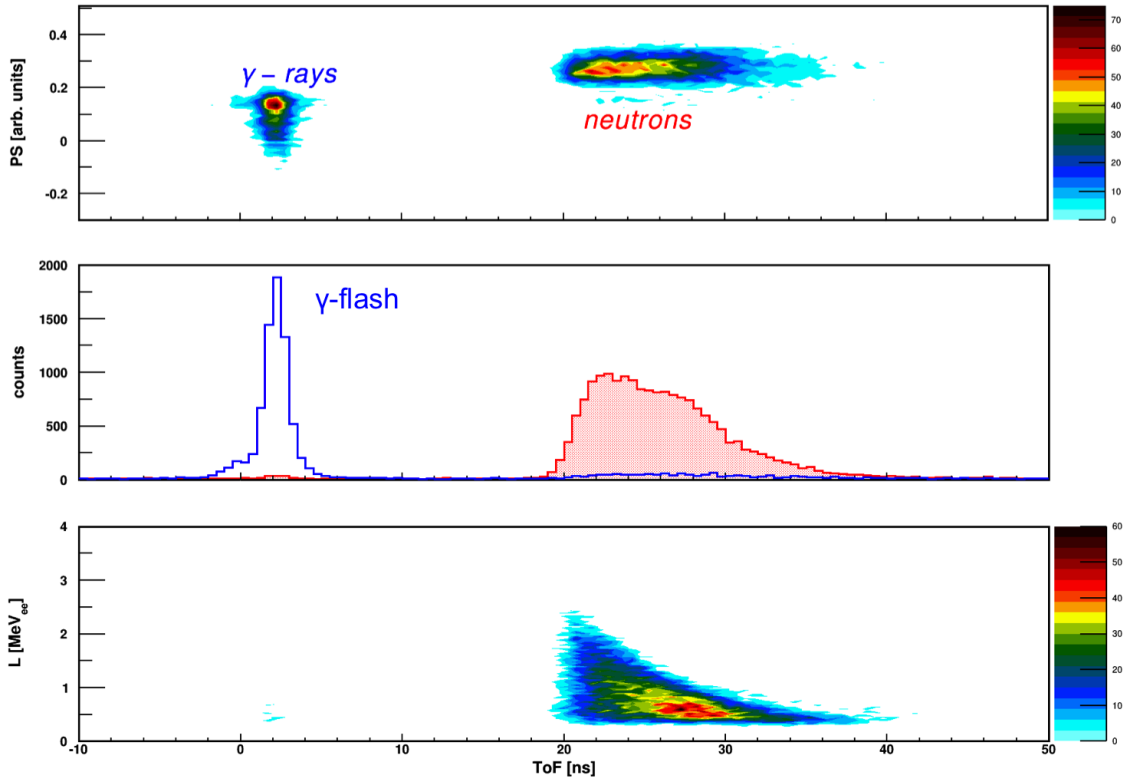

Figure 3.7: The top panel shows a contour plot of PS plotted against TOF. The middle panel shows the TOF spectrum for events identified by PSD as gamma-rays in the non-shaded (blue) histogram and neutrons shaded in red. In the bottom panel, light yield L is plotted against TOF for neutron events identified by PSD.

The tail of events to the right of the gamma-flash corresponds to non-prompt gamma-rays and randoms. The ∼1.8 ns FWHM of the gamma-flash is consistent with the timing jitter on the PMT signals. The broad red shaded peak centered at about 25 ns corresponds to time-correlated 4.44 MeV neutron/gamma-ray pairs where the fast neutron triggered the NE-213 detector while the 4.44 MeV gamma-ray triggered the YAP detector. A neutron with time-of-flight measured in this manner has been "tagged". The very low level background consists of randoms. Random events arose when

the NE-213 detector started the TOF measurement, but no correlated stop was received from the YAP. Typical random events included cosmic rays, room background, Am/Be neutrons not correlated with a 4.44 MeV gamma-ray, and Am/Be neutrons where the 4.44 MeV gamma-ray was missed due to YAP inefficiency or geometry. The bottom panel shows neutron pulse height plotted against TOF in a contour plot. It is obvious that the maximum light yield of neutron-induced recoiling protons is a strong function of the kinetic energy of the incident neutron. The events in the two lower panels were chosen by applying a PS ≥ 0.19 cut.

3.2.2 Neutron Kinetic Energy

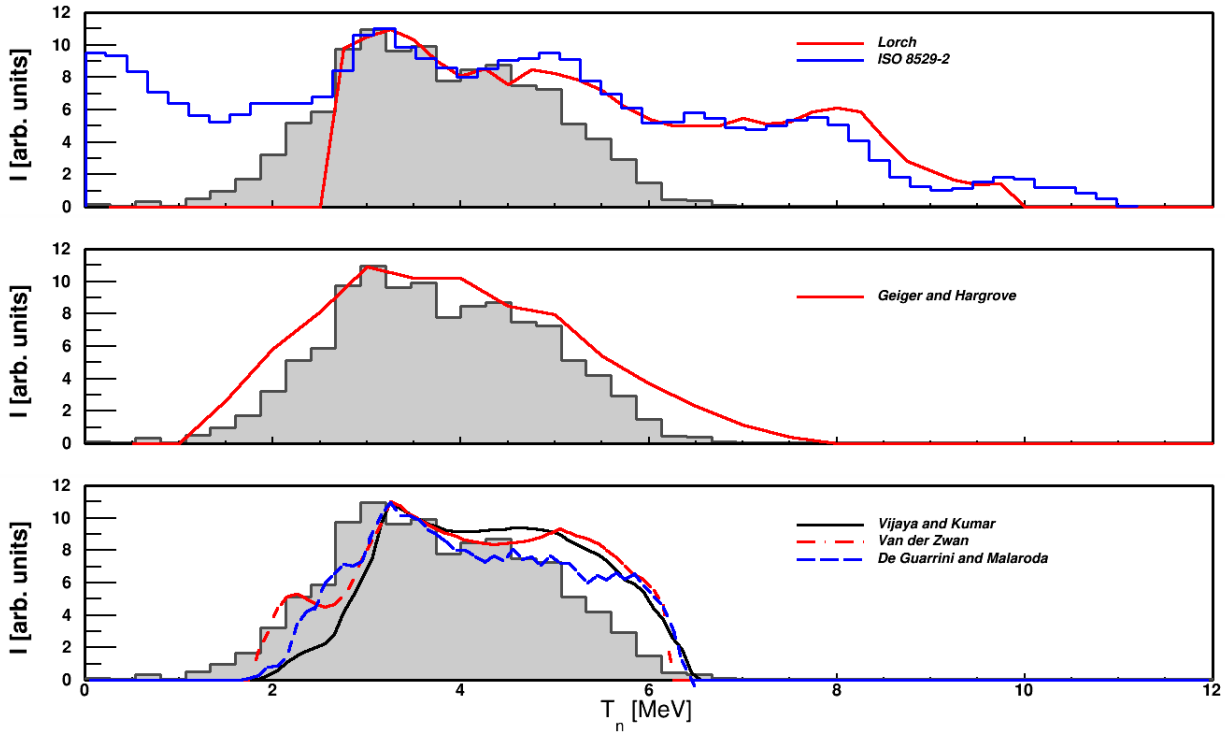

Figure 3.8: The results of this work are presented as the gray histogram in each panel. The top panel shows a measurement by Lorch [20] (red line) and the ISO 8529-2 Am/Be neutron spectrum (blue histogram). The middle panel compares these results with tagged-neutron results obtained by Geiger and Hargrove [52] (red). The bottom panel presents theoretical calculations of the tagged-neutron spectrum [21–23].

For the neutron energy range 2 - 7 MeV, the TOF spectra can be transformed from ns to MeV in the classical approach since the maximum expected neutron speed is less

than 12% of the speed of light.

$$T_n = \frac{1}{2} m_n v^2 = \frac{1}{2} m_n c^2 \beta^2 = \frac{1}{2} m_n c^2 \frac{s^2}{TOF^2 c^2}. \tag{3.3}$$

In Equation 3.3, the kinetic energy T_n is given in MeV, the neutron mass is $m_n = 939.56 \frac{MeV}{c^2}$, s is the distance between the center of detector and the neutron source in meters and TOF is the elapsed time between neutron emission from the source and detection in the detector in ns. The measured tagged-neutron distribution is shown in all three panels in gray. A hardware threshold of 250 keV_{ee} was employed corresponding to a neutron energy of $\sim$1.3 MeV. The measured data are yields and have not been corrected for neutron-detection efficiency or detector acceptance. In all 3 panels, the maximum values of the spectra (at $\sim$3 MeV) have been normalized to the distribution determined in this work. In the top panel, the ISO 8529-2 reference neutron radiation spectrum for Am/Be is shown together with the full-energy neutron spectrum of Lorch [20] which is widely quoted in work with Am/Be sources. The agreement between the tagged data, those of Lorch, and the reference spectrum in the region of overlap (between 2.5 and 5 MeV) is excellent. Agreement between the ISO spectrum and the Lorch data is very good between 2.5 MeV and 10 MeV. The ISO reference spectrum shows some strength above 10 MeV which Lorch did not observe. The tagged-neutron data show no strength above $\sim$7 MeV, since 4.44 MeV are lost to the creation of the de-excitation gamma-ray. This is a purely energetic effect, independent of both acceptance and efficiency effects. The ISO reference spectrum shows considerable strength below 2.5 MeV. The data presented here also show some strength in this region. The Lorch data show a sharp cutoff at about 2.5 MeV, attributed to an analysis threshold cut. A previous tagged-neutron measurement by Geiger and Hargrove [52] is presented in the middle panel. The agreement with the data from this work is very good. The small difference in the strengths observed in the two measurements can be attributed to neutron-detection efficiency, acceptance effects and energy resolution. The bottom panel shows three independent theoretical calculations [21–23]. A detailed discussion of these calculations is beyond the scope of this thesis, but all three distributions are in good agreement with both the new data and each other. It is obvious to conclude that the tagged particles are fast neutrons.

3.2.3 Neutron-Induced Recoil-Proton Light Yield

The neutron-induced recoil-proton light yield was determined by creating pulse-height histograms for incident neutron energies in intervals of 0.2 MeV. Two methods were used to determine the maximum pulse height of the distribution. In the first method, Gaussian functions were fitted to the smeared edges of the neutron pulse-height spectra which arose from resolution effects. The maximum energy was determined in the same way as the position of Compton edge for incident gamma-rays; namely, with the Knox method [51]. Such an approach was first used by Naqvi *et*

al. [53] As an alternative, the first derivatives can be calculated from the smoothed neutron light yield functions. This method was used by Kornilov *et al.* [54] Figure 3.9 shows the neutron-response function for 4.8 MeV incident neutrons as a gray shaded distribution and the first derivative of the function in blue squares to illustrate both approaches.

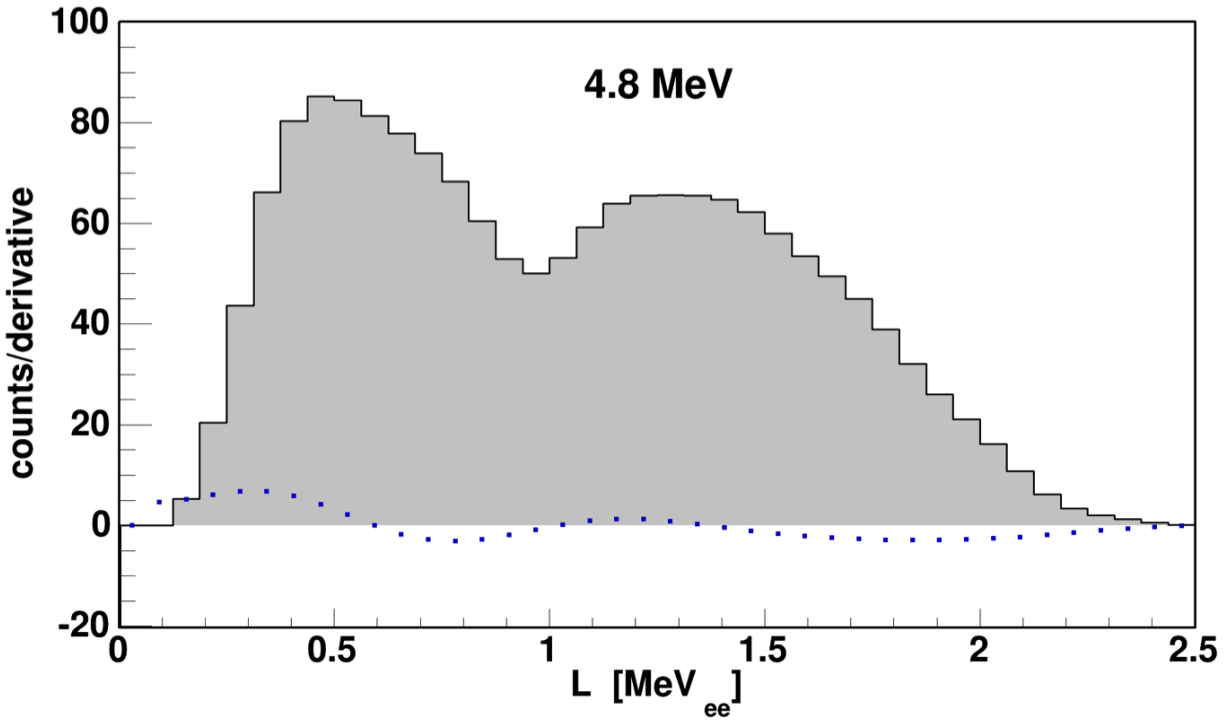

Figure 3.9: The light yield response function (gray shaded) and its first derivative (blue squares) are shown for 4.8 MeV neutrons.

Figure 3.10 shows the measured proton light yield for the NE-213 detector from this work as blue filled squares in the top panel obtained using the Knox-Naqvi method and in the middle panel obtained using the Kornilov method. The results for a LS301[4] detector provided by Scionix [30] (h =50 mm $\times$ d = 100 mm) from [54] are shown as open red triangles in the middle panel. The data of Naqvi *et al.* [53] for a NE-213 detector (h = 50 mm $\times$ d = 50 mm) are shown as red circles in the top panel. The bottom panel shows the ratio of the results calculated with the Kornilov method to the results determined using the Knox-Naqvi method. Good agreement is observed.

To parameterize the proton light yield, a recently suggested empirical function [54]

[4]LS301 is the notation of Scionix for the NE-213 equivalent organic scintillator EJ-301 [32].

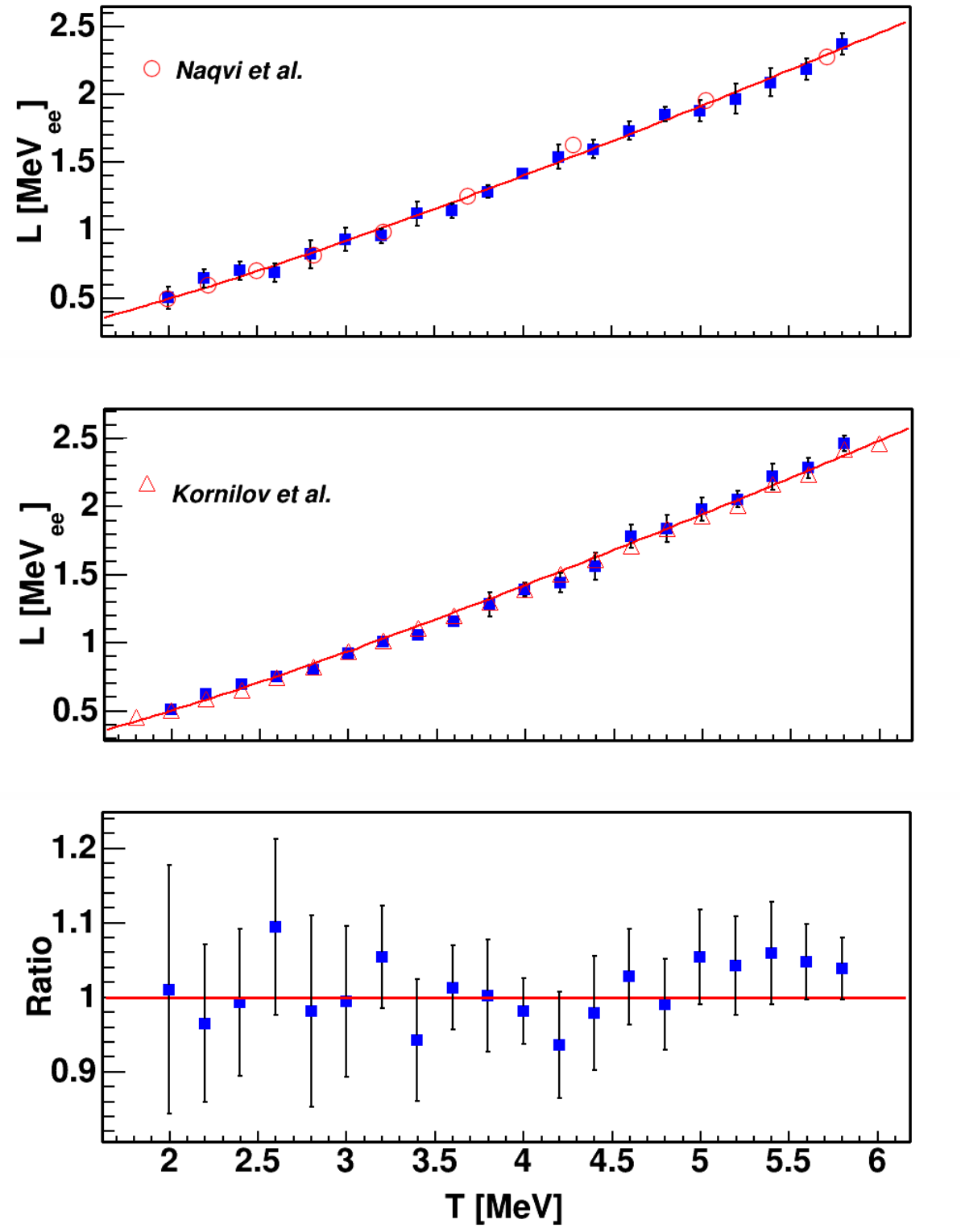

Figure 3.10: Neutron-induced recoil-proton light yield from this work (blue squares) plotted against neutron kinetic energy. Top Panel: Knox-Naqvi method. The open red circles are the original Naqvi *et al.* [53] data. Middle panel: Kornilov method. The open red triangles are the original Kornilov [54] data. Bottom panel: ratio of the light yield obtained with the different methods (Kornilov/Knox-Naqvi) for the data from this work.

was fitted to the data.

$$L_p = L_0 \frac{T_n^2}{T_n + L_1}, \tag{3.4}$$

where L_p is the proton light yield in MeV_{ee}, T_n is the neutron kinetic energy in MeV and L_0 and L_1 are parameters which represent the quenching[5] and the non-linear response of the scintillator to protons in units of $\frac{MeVee}{MeV}$ and MeV respectively. Parameterization is an easy and widely applied method used to deal with quenching and the non-linear response of organic scintillators to ions.

Scintillator		L_0	L_1
NE-213	This Work with Kornilov Method	0.615 ± 0.028	2.92 ± 0.29
NE-213	This Work with Knox-Naqvi Method	0.609 ± 0.051	2.97 ± 0.61
NE-213	Naqvi	0.620 ± 0.035	3.07 ± 0.42
LS301	Kornilov	0.617 ± 0.013	3.02 ± 0.17

Table 3.1: Proton light yield parametrizations for NE-213.

The calculated values agree within statistical errors for both methods, if compared to previous measurements and to each other (see Table 3.1). The parametrization values for both the LS301 detector from Kornilov *et al.* and for the NE-213 detector from Naqvi *et al.* were calculated in this work from data taken from the references and by fitting Equation 3.4 in the same energy range as the measured data.

[5]Quenching refers to a reduced light yield for recoiling protons in liquid scintillator when compared to the light emission induced by recoiling electrons of the same energy.

4 Conclusion and Outlook

This work presents the first steps taken towards the development of a test-bed for fast-neutron irradiation. The test-bed was designed with a focus on detector characterization. Features such as pulse-shape discrimination, pulse-height responses and the linearity of particle-response functions can be established by using either the non-tagged method or the TOF setup. Neutron events may be separated from gamma-ray events using TOF. This allows for detectors without PSD capabilities to be tested.

The need for a facility having these capabilities is obvious and a broad user base from industry, academia and the detector groups of research facilities is anticipated. The test-bed has been developed with generous support of the European Spallation Source ESS AB and a large number of users will come from the ESS Neutron Technology Division, namely the Detector Group and the Neutron Optics and Shielding Group. They are interested in testing equipment, e.g. detectors and beam guides, for both fast-neutron and gamma-ray responses. This is important since the pulse structure of ESS linear accelerator is long and will present new challenges to the required instrumentation [55]. The test-bed has already been used to characterize a commercial detector developed by the Swiss company Arktis Radiation Detectors.

Users from the neutron-scattering community will benefit from an upgrade of the facility which is intended to provide tagged thermal neutrons ($T_n \approx 25$ meV). This upgrade will allow for the simultaneous characterization of detectors for both background signals and event signals, which is currently not possible. Further evaluation includes measurements of absolute detection efficiency using fission fragments from a ^{252}Cf source. The test-bed will also be used to facilitate undergraduate education. Students use the modern equipment for project work next to professional researchers.

Bibliography

[1] United States Committee on Army Science and Technology for Homeland Defense, Board on Army Science and Technology, Division on Engineering and Physical Sciences, National Research Council, Indications and Warn- ing Technologies, in Science and Technology for Army Homeland Security: Report 1, National Academies Press (2003).

[2] W.C. Lyons and G.J. Plisga. *Current practice in well logging, reservoir engineering and secondary recovery. In: The Petroleum Engineering Handbook: Sustainable Operations*. Gulf Publishing Company, 2013.

[3] R. Chandra et al. *IEEE NSS/MIC*, page 508, 2010.

[4] R. Chandra et al. *J. Instrum.*, 7:C03035, 2012.

[5] M.R. Islam and M.I. Kahn. *Drilling and well completions, reservoir engineering. In: Standard Handbook of Petroleum and Natural Gas Engineering*. Gulf Publishing Company, 2011.

[6] A. Tomanin et al. *Nucl. Inst. and Meth. A*, 756(0):45, 2014.

[7] J. Walker. *Phys. Technol.*, 13:239, 1982.

[8] A. Cho. *Science*, 326:778, 2009.

[9] K. Zeitelhack. *Neutron News*, 23(4):10, 2012.

[10] T.M. Persons and G. Aloise. *United States Government Accountability Office GAO-11-753*, 2011.

[11] D. Kramer. *Physics Today*, 64:20, 2011.

[12] R.T. Kouzes. *United States Government Accountability Office GAO-11-753*, 2011.

[13] R. Hall-Wilton et al. *IEEE NSS/MIC*, page 4283, 2012.

[14] O. Kirstein et al. *PoS (Vertex2014)*, page 29, 2014.

[15] M Shoji et al. *J. Instrum.*, 7(05):C05003, 2012.

[16] K. Andersen et al. *Nucl. Inst. and Meth. A*, 720(0):116, 2013.

[17] C.L. Wang et al. *IEEE NSS/MIC*, page 4877, 2011.

[18] Supplied by High Tech Sources Limited, Unit 6, Moorbrook, Southmead, Industrial Estate, Didcot, Oxfordshire, Uk OX11 7HP; http:///www.hightechsource.co.uk/. For details see http:///www.hightechsource.co.uk/Legacy/Resources/Americium-Berryliu.pdf. .

[19] E. Aza et al. *Radiation Measurements*, 61:25, 2014.

[20] E.A. Lorch. *Int. J. Appl. Radiat. Isot.*, 60:959, 1973.

[21] A.D. Vijaya and A. Kumar. *Nucl. Instrum. Methods*, 111:435, 2004.

[22] L. Van der Zwan. *Can. J. Phys.*, 46:1527, 1968.

[23] F. De Guarrini and R. Malaroda. *Nucl. Instrum. Methods*, 92:277, 1968.

[24] A.A. Mowlavi and R. Koohi-Fayegh. *Appl. Radiat. Isot.*, 60:959, 2004.

[25] Liu et al. *Appl. Radiat. Isot.*, 65:1318, 2007.

[26] http://geant4.cern.ch/ .

[27] http://www.fluka.org .

[28] http://www.maxlab.lu.se.

[29] VINK AS. http://www.vink.se.

[30] Scionix Holland BV. http://www.scionix.nl.

[31] Hamamatsu Photonics. http://www.hamamatsu.com/jp/en/R1924.html.

[32] NE213 is no longer produced. Eljen Technologies offers EJ-301 http://www.eljentechnology.com/index.php/products/liquid-scintillators/71-ej-301 while Saint Gobain offers BC-501 http://www.crystals.saint-gobain.com/uploadedFiles/SG-Crystals/Documents/SGC%20BC501_501A_519%20Data%20Sheet.pdf.

[33] http://www.us.schott.com/borofloat/english/index.html for details. Supplied by Glasteknik i Emmaboda AB, Utvägen 6 SE-361 31 Emmaboda, Sweden.

[34] http://www.huntsman.com/advanced_materials/a/Our%20Technologies/Ready%20to%20Use%20Formulated%20Systems/Adhesives.

[35] Viton is a registered tradmark of DuPont Perfomance Elastomers LLC.

[36] http://www.eljentechnology.com/index.php/products/paints/87-ej-520.

[37] Supplied by Nordic Plastics Group AB, Bronsyxegatan 6, SE-213 75 Malmö, Sweden.

[38] http://www.eljentechnology.com/index.php/products/pmma-a-uvt-material/102-light-guides.

[39] http:///www.eljentechnology.com/index.php/products/paints/87-ej-510.

[40] ET Enterprise Ltd. http://www.et-enterprises.com.

[41] http://www.arktis-detectors.com/.

[42] Polytetrafluoroethylene, also known as Teflon; http://www2.dupont.com/TeflonIndustrial/enUS/products/selectionguides/coatings.html.

[43] D.N. McKinsey and otherse. *Nucl. Inst. and Meth. A*, 516(2–3):475, 2004.

[44] Hamamatsu Photonics. http://www.hamamatsu.com/us/en/R580.html.

[45] S. Ritt. *IEEE NSS/MIC*, page 1512, 2008.

[46] https://root.cern.ch.

[47] H. Friederich et al. *IEEE Trans. Nucl. Sci.*, page 1652, 2011.

[48] A. Jhingan et al. *Nucl. Inst. and Meth. A*, 585(3):165, 2008.

[49] *Nucl. Inst. and Meth. A*, 617(1–3):492, 2010.

[50] I.A. Pawełczak et al. *Nucl. Inst. and Meth. A*, 711(0):21, 2013.

[51] H.H. Knox and T.G. Miller. *Nucl. Inst. and Meth.*, 101:519, 1972.

[52] K.W. Geiger and C.K. Hargrove, 1964.

[53] A.A Naqvi et al. *Nucl. Inst. and Meth. A*, 353:156, 1994.

[54] N.V. Kornilov et al. *Nucl. Inst. and Meth. A*, 599:226, 2009.

[55] N Cherkashyna et al. *J. Phys. Con. Ser.*, 528(1):012013, 2014.

Acknowledgments

At the start let me apologize. I most likely excluded a person/persons from these acknowledgments who supported me during the last couple of years or did me another kindness and deserved to be mentioned. This is neither intentional nor is it accidental, but simply unavoidable. I hope you may forgive me.

My first words of gratitude have to go to Dr. Kevin Fissum, my main supervisor. Kevin, thank you for everything. You supplied me with a great opportunity and I could not have done this without you. You always supported me, gave me guidance where needed and let me explore freely when appropriate. Thank you. My second thoughts go to Dr. Richard Hall-Wilton. Thank you Richard for your time and guidance. You had an open door for me, supported me and made time for me in your busy schedule. I hope you know how much I appreciated it. I want to say thank you to both Dr. John Annanad and Dr. Ramsey Al Jebali from the University of Glasgow. John, your help has been invaluable in many an endeavor from simulations to setting up the DAQ. Ramsey, thank you again for your support with the project and for all the nice discussions about physics and life. I thank the European Spallation Source ESS AB for supplying a large part of the funding for my project. I want to say thank you to both the ESS Detector Group and the ESS Neutron-Optic and Shielding Group. All of you have been helpful in one way or another over the last years. I thank the Photonuclear Group and the Radiation Safety Group at the MAX IV Laboratory for their support during the initial test "beamtimes" in the nuclear cave and for giving me access to their Am/Be source. A special thank you goes to Håkan Svensson. You supplied me with the technical drawings for both the water tank and the scintillator detector cells and turned vague ideas into reality. I want to thank all the people at the Division of Nuclear Physics for giving me a warm welcome and supporting me during my work. I thank the Royal Physiographic Society in Lund for their support for new equipment to improve the DAQ system. Finally, I want to thank my family, my parents and siblings. I know I can always count on you.

PAPER I

Applied Radiation and Isotopes 98 (2015) 74–79

Contents lists available at ScienceDirect

Applied Radiation and Isotopes

journal homepage: www.elsevier.com/locate/apradiso

Tagging fast neutrons from an ^{241}Am/^{9}Be source

J. Scherzinger [a,b], J.R.M. Annand [c], G. Davatz [d], K.G. Fissum [a,b,*], U. Gendotti [d], R. Hall-Wilton [b,f], E. Håkansson [a], R. Jebali [d,1], K. Kanaki [b], M. Lundin [e], B. Nilsson [b,e], A. Rosborge [e], H. Svensson [e,g]

[a] Division of Nuclear Physics, Lund University, SE-221 00 Lund, Sweden
[b] Detector Group, European Spallation Source ESS AB, SE-221 00 Lund, Sweden
[c] University of Glasgow, Glasgow G12 8QQ, Scotland, UK
[d] Arktis Radiation Detectors Limited, 8045 Zürich, Switzerland
[e] MAX IV Laboratory, Lund University, SE-221 00 Lund, Sweden
[f] Mid-Sweden University, SE-851 70 Sundsvall, Sweden
[g] Sweflo Engineering, SE-275 63 Blentarp, Sweden

HIGHLIGHTS

- Neutrons emitted from a Be-compound source are tagged.
- The resulting beam of neutrons is continuous and polychromatic.
- The energy of each neutron is known.
- The approach is cost-effective.

ARTICLE INFO

Article history:
Received 15 September 2014
Received in revised form
30 December 2014
Accepted 5 January 2015
Available online 6 January 2015

Keywords:
Americium–beryllium
Gamma-rays
Fast neutrons
Time-of-flight

ABSTRACT

Shielding, coincidence, and time-of-flight measurement techniques are employed to tag fast neutrons emitted from an ^{241}Am/^{9}Be source resulting in a continuous polychromatic energy-tagged beam of neutrons with energies up to 7 MeV. The measured energy structure of the beam agrees qualitatively with both previous measurements and theoretical calculations.

1. Introduction

Fast neutrons are important probes of matter and diagnostic tools (Walker, 1982; United States Committee on Army Science and Technology for Homeland Defense, 2003; http://www.pos.sissa.it/cgi-bin/reader/conf.cgi?confid=25; http://www.hep.lu.se/staff/christiansen/proceeding.pdf; http://www.iopscience.iop.org/1748-0221/focus/extra.proc19; Chandra et al., 2010, 2012; Lyons and Plisga, 2011; Peerani et al., 2012; http://www.plone.esss.lu.se/; Islam and Khan, 2013; Lewis et al., 2013, 2014; Tomanin et al., 2014). Sources of fast neutrons for controlled irradiations include nuclear reactors, particle accelerators, and radioactive sources. Drawbacks associated with nuclear reactors and particle accelerators include their accessibility and availability, as well as the very high cost per neutron. In contrast, radioactive sources provide neutrons with a substantially lower cost per neutron. Drawbacks associated with radioactive sources include the complex mixed field of radioactive decay products which complicate the experimental situation. As a first step towards developing a source-based fast-neutron irradiation facility, we have employed well-understood shielding, coincidence, and time-of-flight (TOF) measurement techniques to attenuate and subsequently unfold the mixed decay-product radiation field provided by an ^{241}Am/^{9}Be (hereafter referred to as Am/Be) source, resulting in a polychromatic energy-tagged neutron beam.

* Corresponding author at: Division of Nuclear Physics, Lund University, SE-221 00 Lund, Sweden. Fax: +46 46 222 4709.
E-mail address: kevin.fissum@nuclear.lu.se (K.G. Fissum).
[1] Present address: University of Glasgow, Glasgow G12 8QQ, Scotland, UK.

http://dx.doi.org/10.1016/j.apradiso.2015.01.003
0969-8043/

2. Apparatus

2.1. Am/Be source

The heart of the irradiation facility consists of a (nominal) 18.5 GBq Am/Be radioactive source (https://www.hightechsource.co.uk/). This source is a mixture of americium oxide and beryllium metal contained in an X.3 capsule[2] (see Fig. 1).

Radioactive ^{241}Am has a half-life of 432.2 years and decays via α emission (five different energies averaging ~5.5 MeV) to ^{237}Np. The dominant energy of the resulting background gamma-rays from the decay of the intermediate excited states in ^{237}Np is ~60 keV. ^{237}Np has a half-life of over 2 million years. ^{9}Be is stable.

Fast neutrons are produced when the decay α particles interact with ^{9}Be. Depending on the interaction and its kinematics, ^{12}C and a free neutron may be produced. The resulting free-neutron distribution has a maximum value of about 11 MeV and a substructure of peaks whose energies and relative intensities vary depending upon the properties of the Am/Be source containment capsule and the size of the $^{241}AmO_2$ and Be particles in the powders employed – see the detailed discussion presented in Lorch (1973). In general, approximately ~25% of the neutrons emitted have an energy of less than ~1 MeV with a mean energy of ~400 keV (https://www.hightechsource.co.uk/). The average fast-neutron energy is ~4.5 MeV. Both the gamma-ray and neutron dose rates at a distance of 1 m from our unshielded source in the X.3 capsule were measured to be 11 μSv/h, for a total unshielded dose rate of 22 μSv/h. The unshielded source has been independently determined to emit $(1.106 \pm 0.015) \times 10^6$ neutrons per second nearly isotropically (National Physical Laboratory, 2012).

The kinematics and the reaction cross section for the ^{9}Be(α, n) interaction determine the state of the recoiling ^{12}C nucleus produced in the reaction. The calculations of Vijaya and Kumar (1973) (for example) suggest that the relative populations of the ground/first/second excited states for the recoiling ^{12}C nucleus are ~35%/ ~ 55%/ ~ 15%. If the recoiling ^{12}C nucleus is left in its first excited state, it will promptly decay to the ground state via the isotropic emission of a 4.44 MeV gamma-ray. Mowlavi and Koohi-Fayegh (2004) as well as Liu et al. (2007) have measured R, the 4.44 MeV γ-ray to neutron ratio for Am/Be, to be approximately 0.58. Again, this is seemingly dependent upon the Am/Be capsule in question. Regardless, almost 60% of the neutrons emitted by an Am/Be source are accompanied by a prompt, time-correlated 4.44 MeV γ-ray. We exploit this property of the source to determine neutron TOF and thus kinetic energy by measuring the elapsed time between the detection of the 4.44 MeV γ-rays and the detection of the fast neutrons. Note that by employing this technique, we necessarily restrict our available "tagged" neutron energies to a maximum value of ~7 MeV as 4.44 MeV of the reaction Q-value are "lost" to the de-excitation gamma-ray.

2.2. YAP:Ce 4.44 MeV gamma-ray trigger detectors

The 2 YAP:Ce[3] fast (~5 ns risetime) gamma-ray trigger detectors (hereafter referred to as YAPs) were provided by Scionix (http://www.scionix.nl). A detector (see Fig. 2) consisted of a cylindrical 1 in (diameter) × 1 in (height) YAP crystal (Moszyński et al., 1998) coupled to a 1 in Hamamatsu Type R1924 photomultiplier tube (PMT) (http://www.hamamatsu.com) operated at about −800 V. Gains for the YAP detectors were set using a YAP event trigger and standard gamma-ray sources. Typical energy resolution obtained for the 662 keV peak of ^{137}Cs using such a detector was about 10%. YAP:Ce is radiation hard and quite insensitive to neutrons of all energies, which makes it ideal for detecting gamma-rays within the large fast-neutron field of the Am/Be source. We stress that because of their small volume, the YAP detectors were not used for spectroscopy, but simply to trigger on any portion of the energy deposited by the 4.44 MeV gamma-rays emitted by the source. A 3 mm thick Pb sleeve placed around the source (see Section 2.4) to attenuate the high intensity 60 keV gamma-ray field and a 350 keV_{ee} discriminator threshold proved to be an effective combination for the YAP detection of these 4.44 MeV gamma-rays.

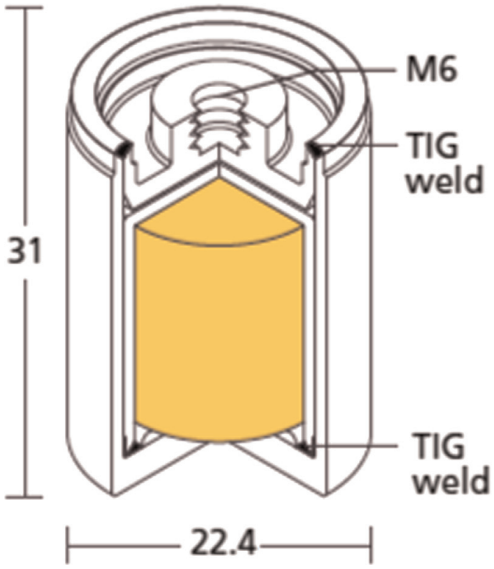

Fig. 1. The Am/Be source (figure from https://www.hightechsource.co.uk/). Dimensions in mm. The yellow shaded volume at the central core of the capsule corresponds to the Am/Be. (For interpretation of the references to color in this figure caption, the reader is referred to the web version of this article.)

Fig. 2. Photograph of a YAP detector. A 1 in (diameter) × 1 in (height) crystal has been mounted on a 1 in (diameter) × 10 cm (length) PMT.

2.3. NE-213 fast-neutron and gamma-ray liquid-scintillator detector

The NE-213 fast-neutron and gamma-ray detector employed in this work is shown in Fig. 3. A 3 mm thick cylindrical aluminum cell with a depth of 62 mm and a diameter of 94 mm housed the NE-213. The inside of the cell was treated with xylene-solvent withstanding EJ-520 (http://www.eljentechnology.com/index.php/products/paints/87-ej-520) titanium dioxide reflective paint. The cell was sealed with a 5 mm thick borosilicate glass plate (http://

[2] An X.3 capsule is a tig-welded, double-layered, stainless-steel cylinder approximately 30 mm (height) × 22 mm (diameter).

[3] YAP:Ce stands for yttrium aluminum perovskite:cerium ($YAlO_3$, Ce^+ doped).

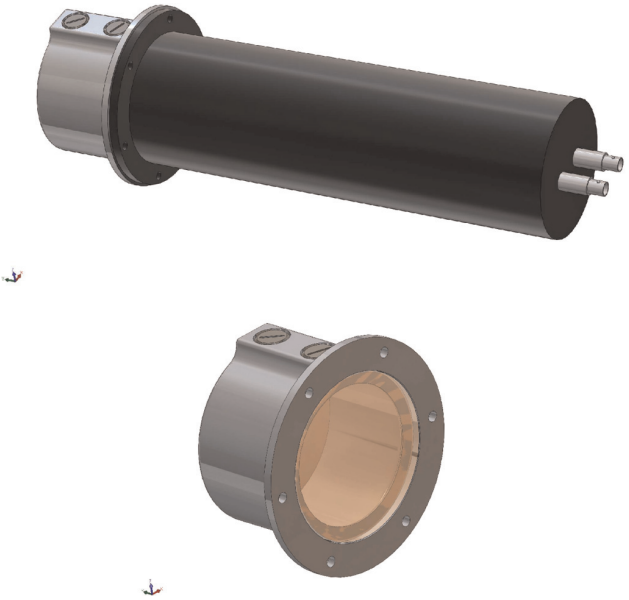

Fig. 3. CAD drawing of the NE-213 detector. Top panel: the detector. The large black cylinder to the right is the magnetically shielded 3 in ET Enterprises 9821KB photomultiplier-tube assembly. The small gray cylinder to the left contains the NE-213. Bottom panel: an enlargement of the small gray cylinder "cup". The screws on top allow for the filling or draining of the liquid cylinder. A borosilicate-glass window (light brown) serves as the optical boundary. (For interpretation of the references to color in this figure caption, the reader is referred to the web version of this article.)

www.us.schott.com/borofloat/english/index.html) attached using Araldite 2000+ glue, which is highly resistant to both temperature and chemicals. The penetrations into the cell were closed with M-8 threaded aluminum plugs with 20 mm diameter heads and sealed with 14 mm diameter Viton O-rings. The assembled cell was filled with the nitrogen-flushed NE-213 using a nitrogen gas-transfer system.

After the cell was filled, the borosilicate glass window was coupled to a cylindrical PMMA UVT lightguide with a height of 57 mm and a diameter of 72.5 mm. The lightguide wall was painted with water-soluble EJ-510 (http://www.eljentechnology.com/index.php/products/paints/86-ej-510) reflective paint. The lightguide was then pressure-coupled to a spring-loaded, magnetically shielded 3 in ET Enterprises 9821KB PMT assembly (www.et-enterprises.com/files/file/Pmtbrochure11.pdf) operated at about −2000 V. In order to ensure the reproducibility of the behavior of the detector over an extended period of time rather than maximize light transmission, optical grease was not used in the assembly. Gain for the NE-213 detector was set using an NE-213 detector event trigger and a set of standard gamma-ray sources together with the prescription of Knox and Miller (1972).

2.4. Configuration

A block diagram of the experiment configuration is shown in Fig. 4. The Am/Be source was placed so that its cylindrical-symmetry axis corresponded to the vertical direction in the lab at the center of a 3 mm thick cylindrical Pb sleeve (with the same orientation) to attenuate the 60 keV gamma-rays associated with the decay of ^{241}Am.[4] A YAP detector was placed with its crystal approximately 5 cm from the Am/Be source at source height. The crystal orientation was such that its cylindrical symmetry axis also

[4] The half-value layer for Pb for 60 keV gamma-rays is <1 mm.

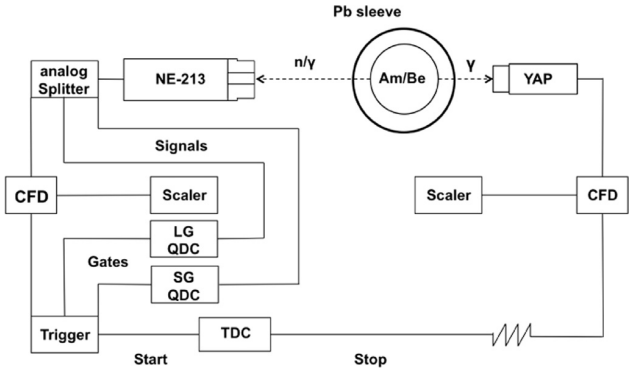

Fig. 4. A simplified overview of the experimental setup (not to scale). The Am/Be source, the Pb sleeve, a single YAP detector, and a NE-213 detector are all shown together with a block electronics diagram.

corresponded to the vertical direction in the lab. This detector triggered overwhelmingly on the 4.44 MeV gamma-rays radiating from the source which came from the decay of the first excited state of ^{12}C. A NE-213 detector was placed approximately 68 cm from the Am/Be source at source height. The cylindrical symmetry axis of the NE-213 detector pointed directly at the center of the source. This detector triggered on both 4.44 MeV gamma-rays and fast neutrons coming from the source, as well as cosmic rays and room background.[5]

2.5. Electronics and data acquisition

The analog signals from the YAP trigger detector and the NE-213 detector were passed to LRS 2249A and 2249W CAMAC charge-to-digital converters (QDCs) and PS 715 NIM constant-fraction (timing) discriminators. The resulting logic signals from the discriminators were passed to LRS 2228A CAMAC time-to-digital converters (TDCs) and LRS 4434 scalers. These signals were recorded on an event-by-event basis for offline processing using a LINUX PC-based data-acquisition (DAQ) system exploiting the ROOT (Brun and Rademakers, 1997) data-analysis framework. Connections to VME and CAMAC crates were respectively facilitated by a SBS 616 PCI-VME bus adapter and a CES 8210 CAMAC branch driver. In YAP calibration mode, signals from a YAP detector were periodically employed to trigger the DAQ and thus monitor the gains of the YAP detectors. In TOF mode, signals from the NE-213 detector were used to trigger the DAQ so that the gain of the NE-213 detector was continuously monitored. The NE-213 detector QDCs included a 60 ns short-gated (SG) QDC and a 500 ns long-gated (LG) QDC, both of which opened 25 ns before the analog pulse arrived. The NE-213 detector also provided the start trigger for the TOF TDC. The YAP trigger provided the stop trigger for the TOF TDC. By triggering our data-acquisition system on the NE-213 detector, we avoided unnecessary deadtime processing events seen only by the YAPs. Two particular source-related occurrences were of special interest: (1) a fast neutron detected in the NE-213 detector starting the TOF TDC with the corresponding 4.44 MeV gamma-ray detected in the YAP detector stopping it; and (2) prompt, time-correlated gamma-ray pairs emitted from the source being detected in coincidence in the NE-213 and YAP detectors (see below).

[5] Room background consisted primarily of 2.23 MeV gamma-rays associated with neutron capture on the hydrogen in the water and paraffin used as general radiation shielding about the source.

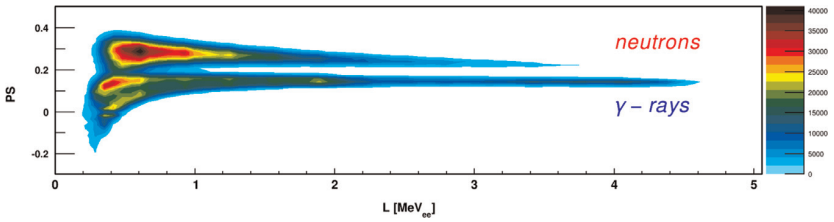

Fig. 5. A contour plot of pulse shape (PS) versus total energy deposited in the LG QDC (L) for correlated fast-neutron/gamma-ray events in the NE-213 detector. The upper distribution corresponds to neutrons while the lower band corresponds to gamma-rays.

3. Results

Fig. 5 shows a contour plot of the energy deposited in the NE-213 detector as a function of "pulse shape" (PS, see below) versus "L" (the energy deposited in the LG QDC). PS was calculated using the "tail-to-total" method (Jhingan et al., 2008; Lavagno et al., 2010; Paweczak et al., 2013); namely, the difference in the energies registered by the LG and SG QDCs was normalized to the energy registered by the LG QDC. As the NE-213 scintillator responded differently[6] to gamma-ray and fast-neutron events, the two distinct distributions appeared in the PS versus L contour plot. Particle identification (PID) based solely upon the pulse-shape discrimination (PSD) characteristics of the NE-213 detector was good, although some overlap between the distributions existed in the vicinity of PS ~ 0.2.

Fig. 6 presents the time-of-flight distribution of the data shown in Fig. 5. No software cut on L was applied in mapping the data from Figs. 5 and 6. The hardware threshold was 250 keV$_{ee}$. The top panel shows a contour plot of PS versus time-of-flight. Time-of-flight based PID is clearly excellent. The bottom panel shows the projection of events from the top panel onto the time-of-flight axis subject to a PS = 0.19 cut to separate neutrons from gamma-rays. The sharp (blue) unshaded peak centered at about 2 ns is known as the "γ-flash".[7] The gamma-flash corresponds to a pair of prompt, time-correlated gamma-rays produced in the source which triggered both the NE-213 detector and the YAP detector. The ~1.8 ns FWHM of the gamma-flash is consistent with the timing jitter on our PMT signals. The tail of events to the right of the gamma-flash corresponds to non-prompt gamma-rays[8] and randoms (see below). The broad (red) shaded peak centered at about 25 ns corresponds to time-correlated 4.44 MeV gamma-ray/fast-neutron pairs where the fast neutron triggered the NE-213 detector while the 4.44 MeV gamma-ray triggered the YAP detector. A neutron with time-of-flight measured in this manner has been tagged. The very low level of background consists of randoms. Random events arose when the NE-213 detector started the time-of-flight measurement, but no correlated stop was received from the YAP. Typical random events included cosmic rays, room background, Am/Be neutrons not correlated with a 4.44 MeV gamma-ray, and Am/Be neutrons where the 4.44 MeV gamma-ray was missed due to YAP inefficiency or geometry.

Fig. 7 shows our tagged-neutron results together with previous results, the ISO 8529-2 reference neutron radiation spectrum for Am/Be,[9] and theoretical calculations. Our data represent yield – they have not been corrected for neutron-detection efficiency or detector acceptance. In all three panels, the maximum values of the spectra at ~3 MeV have been normalized to our distribution. The reference neutron radiation spectrum is shown in the top panel together with the full-energy neutron spectrum of Lorch (1973) which is widely quoted in conjunction with work with Am/Be sources. Agreement between the Lorch data and the reference spectrum is very good between 2.5 MeV and 10 MeV. The reference spectrum shows some strength above 10 MeV which Lorch did not observe. Our data show no strength above ~7 MeV due to the neutron-tagging procedure – 4.44 MeV potentially available to the neutron are "lost" to the creation of the de-excitation gamma-ray. This is neither an acceptance nor an efficiency effect, it is purely energetics. The reference spectrum shows considerable strength below 2.5 MeV. Our data also show some strength in this region. The Lorch data do not. The sharp cutoff at about 2.5 MeV in the Lorch data is not directly discussed in the reference, but based upon its appearance in spectra from several different sources all measured with the same apparatus, we attribute it to an analysis threshold cut as it lies well above their quoted neutron-detector threshold of 1 MeV. Our hardware threshold was 250 keV$_{ee}$ corresponding to a neutron energy of ~1.3 MeV, and no analysis threshold cut was employed. The agreement between our data, those of Lorch, and the reference spectrum between 2.5 and 5 MeV (in the region of overlap) is excellent. The method of tagging the 4.44 MeV de-excitation gamma-ray and a comparable Am/Be source[10] were employed by Geiger and Hargrove (1964) in obtaining the results shown in the middle panel. Both the neutrons and the gamma-rays from their source were detected in Naton 136 plastic scintillators. Agreement with our results is very good. We attribute the small difference in the strengths observed in the two measurements to neutron-detection efficiency and acceptance effects which we do not consider. We attribute the relative broadening of their measured neutron distribution with respect to ours to their quoted poorer than 12% energy resolution for neutron detection, which based on the numbers quoted in their manuscript, we gather was calculated at 2 MeV. At 2 MeV, based upon our gamma-flash FWHM of 1.8 ns, time-of-flight path length of 0.675 m, and detector half-depth of 3.1 cm, our energy resolution was 11%. At 4 MeV, our energy resolution was 19%. The three independent theoretical calculations of the tagged-neutron yield shown in the bottom panel come from Vijaya and Kumar (1973), Van der Zwan (1968), and De Guarrini and Malaroda (1971). The details of these calculations are beyond the scope of this paper, but clearly all three are in reasonable agreement both with each other as well as our results. We conclude we are tagging neutrons.

4. Summary

We have employed shielding, coincidence, and time-of-flight measurement techniques to tag fast neutrons emitted from an Am/

[6] In the liquid scintillator NE-213, gamma-ray scintillations are fast while neutron-associated scintillations have pronounced slow components. Analysis of the time structure of the scintillation components leads to particle identification (PID) and is known as pulse-shape discrimination (PSD).

[7] The instant of the production in the source of the correlated pair of events which produce the time-of-flight data is known as "T_0" and is located at a time-of-flight of 0 ns.

[8] A non-prompt gamma-ray can result from inelastic neutron scattering.

[9] While we employ the reference spectrum in our discussion of results, the interested reader may refer to Marsh et al. (1995) and Chen et al. (2014).

[10] Their source capsule was slightly smaller and emitted about 50% more neutrons per second.

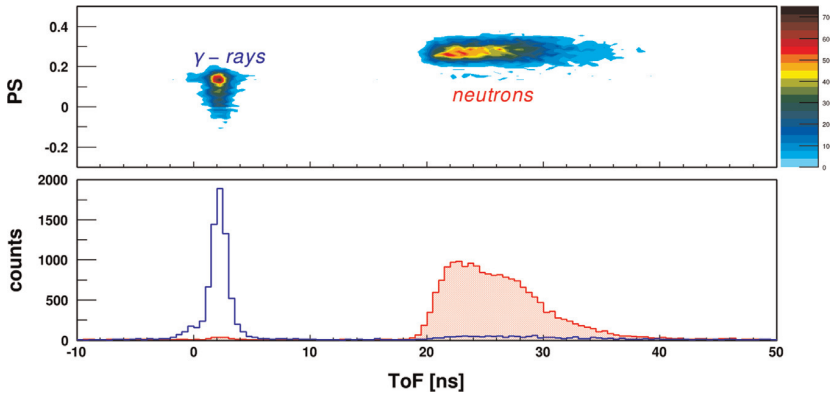

Fig. 6. Time-of-flight distributions. The top panel shows a contour plot of PS versus time-of-flight (ToF). The bottom panel shows the projection of events from the top panel onto the time-of-flight axis. Events identified as gamma-rays in Fig. 5 (the γ-flash) are presented in the sharp (blue) unshaded histogram, while events identified as neutrons are presented in the (red) shaded histogram. (For interpretation of the references to color in this figure caption, the reader is referred to the web version of this article.)

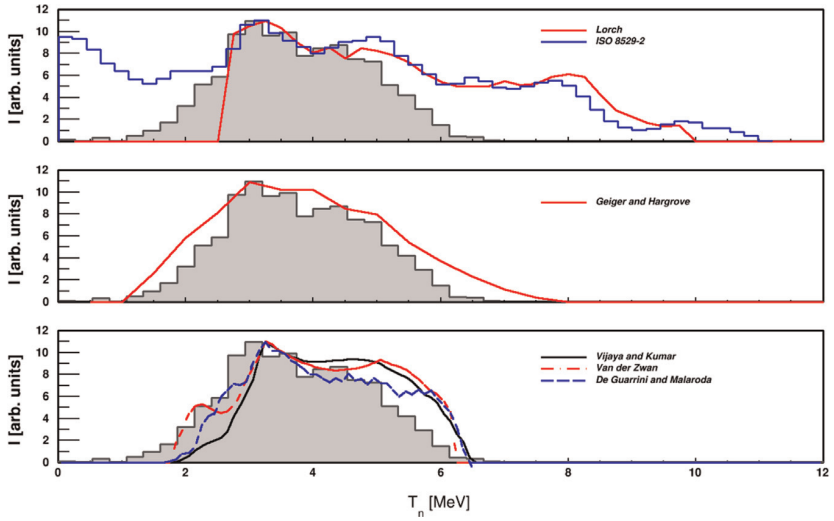

Fig. 7. Our results (the gray shaded histogram) and comparisons. Top panel: the full-energy neutron spectrum (red line) of Lorch (1973) and the ISO 8529-2 reference neutron radiation spectrum for Am/Be (blue open histogram). Middle panel: tagged-neutron results obtained by Geiger and Hargrove (1964) (red line). Bottom panel: theoretical calculations of the tagged-neutron spectrum. The solid black line represents the calculation of Vijaya and Kumar (1973), the red dashed line represents the calculation of Van der Zwan (1968), and the blue dot-dashed line represents the calculation of De Guarrini and Malaroda (1971). (For interpretation of the references to color in this figure caption, the reader is referred to the web version of this article.)

Be source as a first step towards developing a source-based fast-neutron irradiation facility. The resulting continuous polychromatic energy-tagged neutron beam has a measured energy structure that agrees qualitatively with both previous measurements and theoretical calculations. We conclude that our approach works as expected, and anticipate that it can provide a cost-effective means for detector characterization and tests of shielding. We note that this technique will work equally well for all Be-compound neutron sources.

Acknowledgments

We thank the Photonuclear Group at the MAX IV Laboratory for providing access to their experimental hall and Am/Be source. We acknowledge the support of the UK Science and Technology Facilities Council (Grant nos. STFC 57071/1 and STFC 50727/1).

References

Araldite is a Registered Trademark of Huntsman. ⟨http://www.araldite2000plus.com⟩.

Brun, R., Rademakers, F., 1997. ROOT—an object oriented data analysis framework. In: Proceedings AIHENP'96 Workshop, Lausanne, September 1996; Nucl. Instrum. Methods Phys. Res. A 389, 81–86. See also ⟨http://root.cern.ch/⟩.

Chandra, R., Davatz, G., Gendotti, U., Howard, A., 2010. IEEE NSS/MIC, 508.

Chandra, R., Davatz, G., Friederich, H., Gendotti, U., Murer, D., 2012. J. Instrum. 7, C03035.

Chen, Y., Chen, X., Lei, J., An, L., Zhang, X., Shao, J., Zheng, P., Wang, X., 2014. Science China Physics. Mech. Astron. 57, 1885.

De Guarrini, F., Malaroda, R., 1971. Nucl. Instrum. Methods 92, 277.

Geiger, K.W., Hargrove, C.K., 1964. Nucl. Phys. 53, 204.

Hamamatsu Photonics. ⟨http://www.hamamatsu.com⟩.

Supplied by High Tech Sources Limited, Unit 6, Moorbrook, Southmead, Industrial Estate, Didcot, Oxfordshire, UK OX11 7HP; ⟨https://www.hightechsource.co.uk/⟩ For details see ⟨www.hightechsource.co.uk/Legacy/Resources/Americium-Beryllium.pdf⟩.

⟨http://www.eljentechnology.com/index.php/products/paints/86-ej-510⟩.

⟨http://www.eljentechnology.com/index.php/products/paints/87-ej-520⟩.

⟨www.et-enterprises.com/files/file/Pmtbrochure11.pdf⟩ for details.

Proceedings from the Workshop on Neutron, Neutrino, Nuclear, Muon and Medical Physics at ESS, Lund, Sweden, 2009. ⟨http://www.hep.lu.se/staff/christiansen/proceeding.pdf⟩.

Second International Workshop on Fast Neutron Detectors and Applications (FNDA2011), Kibbutz Ein Gedi, Israel, 2011. J. Instrum. 7C (2012). ⟨http://iopscience.iop.org/1748-0221/focus/extra.proc19⟩.

Workshop on Fast Neutron Applications at Spallation Sources, Abingdon, UK, 2013. ⟨http://plone.esss.lu.se/⟩.

International Workshop on Fast Neutron Detectors and Applications (FNDA2006), University of Capetown, South Africa (2006). Proceedings of Science

(FNDA2006). ⟨http://pos.sissa.it/cgi-bin/reader/conf.cgi?confid=25⟩.
⟨http://www.us.schott.com/borofloat/english/index.html⟩ for details. Supplied by Glasteknik i Emmaboda AB, Utvägen 6 SE-361 31 Emmaboda, Sweden.
Islam, M.R., Khan, M.I., 2013. Current practice in well logging, reservoir engineering and secondary recovery. In: The Petroleum Engineering Handbook: Sustainable Operations. Gulf Publishing Company, Houston, Texas (an imprint of Elsevier).
Jhingan, A., Singh, H., Singh, R.P., Golda, K.S., Sugathan, P., Mandal, S., Bhowmik, R.K., 2008. Nucl. Instrum. Methods Phys. Res. A 585, 165.
Knox, H.H., Miller, T.G., 1972. Nucl. Instrum. Methods 101, 519.
Lavagno, A., Gervino, G., Marino, C., 2010. Nucl. Instrum. Methods Phys. Res. A 617, 492.
Lewis, J.M., Raetz, D., Murer, D., Jordan, K.A., 2013. Third International Conference on Advancements in Nuclear Instrumentation Measurement Methods and their Applications, Marseille, France. ⟨http://ieeexplore.ieee.org/stamp/stamp.jsp?tp=&arnumber=6728031⟩.
Lewis, J.M., Kelley, R.P., Murer, D., Jordan, K.A., 2014. Appl. Phys. Lett. 105, 014102.
Liu, Zhenzhou, Chen, Jinxiang, Zhu, Pei, Li, Yongming, Zhang, Guohui, 2007. Appl. Radiat. Isot. 65, 1318.
Lorch, E.A., 1973. Int. J. Appl. Radiat. Isot. 24, 585.
Lyons, W.C. Plisga, G.J., 2011. Drilling and well completions, reservoir engineering. In: Standard Handbook of Petroleum and Natural Gas Engineering, 2nd ed., Gulf Publishing Company, Houston, Texas (an imprint of Elsevier).
Marsh, J.W., Thomas, D.J., Burke, M., 1995. Nucl. Instrum. Methods Phys. Res. A 366, 340.
Moszyński, M., Kapustab, M., Wolski, D., Klamra, W., Cederwall, B., 1998. Nucl. Instrum. Methods Phys. Res. A 404, 157.
Mowlavi, A.A., Koohi-Fayegh, R., 2004. Appl. Radiat. Isot. 60, 959.
Testing performed at National Physical Laboratory, Teddington, Middlesex, UK TW11 0LW on 24 January 2012.
NE-213 is no longer produced. Eljen Technologies offers EJ-301 (http://www.eljentechnology.com/index.php/products/liquid-scintillators/71-ej-301) while Saint Gobain offers BC-501 ⟨http://www.detectors.saint-gobain.com/uploadedFiles/SGdetectors/Documents/Product_Data_Sheets/BC501-501A-519-Data-Sheet.pdf⟩.
Paweczak, I.A., Ouedraogo, S.A., Glenn, A.M., Wurtz, R.E., Nakae, L.F., 2013. Nucl. Instrum. Methods Phys. Res. A 711, 21.
Peerani, P., Tomanin, A., Pozzi, S., Dolan, J., Miller, E., Flaska, M., Battaglieri, M., De Vita, R., Ficini, L., Ottonello, G., Ricco, G., Dermody, G., Giles, C., 2012. Nucl. Instrum. Methods Phys. Res. A 696, 110.
Poly(methyl-methacrylate), also known as acrylic, plexiglass, and lucite. Supplied by Nordic Plastics Group AB, Bronsyxegatan 6, SE-213 75 Malmö, Sweden.
Scionix Holland BV. ⟨http://www.scionix.nl⟩.
Tomanin, A., Paepen, J., Schillebeeckx, P., Wynants, R., Nolte, R., Lavietes, A., 2014. Nucl. Instrum. Methods Phys. Res. A 756, 45.
United States Committee on Army Science and Technology for Homeland Defense, 2003. Board on Army Science and Technology, Division on Engineering and Physical Sciences, National Research Council, Indications and Warning Technologies, in Science and Technology for Army Homeland Security: Report 1. National Academies Press, Washington, DC.
Van der Zwan, L., 1968. Can. J. Phys. 46, 1527.
Vijaya, A.D., Kumar, A., 1973. Nucl. Instrum. Methods 111, 435.
Viton is a Registered Trademark of DuPont Performance Elastomers LLC.
Walker, J., 1982. Phys. Technol. 13, 239.

PAPER II

A First Comparison of the responses of a ^{4}He-based fast-neutron detector and a NE-213 liquid-scintillator reference detector

R. Jebali[a,1], J. Scherzinger[b,d], J.R.M. Annand[c], R. Chandra[a], G. Davatz[a], K.G. Fissum[b,d,*], H. Friederich[a], U. Gendotti[a], R. Hall-Wilton[d,f], E. Håkansson[b], K. Kanaki[d], M. Lundin[e], D. Murer[a], B. Nilsson[d,e], A. Rosborg[e], H. Svensson[e,g], Your Name[h]

[a] *Arktis Radiation Detectors Limited, 8045 Zürich, Switzerland*
[b] *Division of Nuclear Physics, Lund University, SE-221 00 Lund, Sweden*
[c] *University of Glasgow, Glasgow G12 8QQ, Scotland, UK*
[d] *Detector Group, European Spallation Source ESS AB, SE-221 00 Lund, Sweden*
[e] *MAX IV Laboratory, Lund University, SE-221 00 Lund, Sweden*
[f] *Mid-Sweden University, SE-851 70 Sundsvall, Sweden*
[g] *Sweflo Engineering, SE-275 63 Blentarp, Sweden*
[h] *Your Institution*

Abstract

A first comparison has been made between the pulse-shape discrimination characteristics of a novel ^{4}He-based pressurized scintillation detector and a NE-213 liquid-scintillator reference detector using an Am/Be mixed-field neutron and gamma-ray source and a high-resolution scintillation-pulse digitizer. In particular, the capabilities of the two fast neutron detectors to discriminate between neutrons and gamma-rays were investigated. The NE-213 liquid-scintillator reference cell produced a wide range of scintillation-light yields in response to the gamma-ray field of the source. In stark contrast, the ^{4}He-based detector registered a maximum scintillation-light yield of 750 keV$_{ee}$ to the same gamma-ray field. Pulse-shape discrimination for particles with scintillation-light yields of more than 750 keV$_{ee}$ was excellent in the case of the ^{4}He-based detector, and above 750 keV$_{ee}$ its signal was unambiguously neutron.

Keywords: ^{4}He, NE-213, scintillation, gamma-rays, fast neutrons, digitizer, pulse-shape discrimination

*Corresponding author. Telephone: +46 46 222 9677; Fax: +46 46 222 4709
Email address: kevin.fissum@nuclear.lu.se (K.G. Fissum)
[1] present address: University of Glasgow, Glasgow G12 8QQ, Scotland, UK

1. Introduction

Fast neutrons are important both as probes of matter and as diagnostic tools [1–14]. In the case that information about the energy and emission time of a neutron is available, conclusions about its origin can be drawn. The timing precision required to obtain this information may only be provided by neutron detectors that are fast, providing signals with short risetimes. Today, organic liquid scintillators are the detectors-of-choice for fast neutrons. Drawbacks associated with these scintillators are their toxicity, reactive nature, and sensitivity to a broad range of gamma-ray energies.

Scintillators are substances which emit light when subjected to ionizing radiation. The characteristic time constant associated with the light emitted is a function of the properties of the scintillator in question. Certain scintillators respond to different types of ionizing radiation differently; that is, the time constant of the emitted light is different depending upon the density of ionization produced by the incident radiation. Normally, there are several components with different time constants. The relative intensity of these components affects the effective integrated time constant. By carefully analyzing the behavior of the scintillation light as a function of time, one can determine the incident particle type. This procedure is called pulse-shape discrimination (PSD). PSD is often used to distinguish between different types of uncharged particles, namely gamma-rays and neutrons. In scintillators with good PSD properties, incident gamma-rays interact primarily with the atomic electrons of the scintillator, producing close to minimum-ionizing electrons which give a fast (decay times of some 10s of ns) flash of light. On the other hand, incident neutrons interact primarily with the hydrogen in liquid scintillators and ^{4}He nuclei in noble-gas scintillators via scattering, transferring some of their energy. For hydrogen, this energy transfer can be 100%, while for ^{4}He, the energy transfer is at best 64%. The resulting flashes of light arising from the much denser ionization produced by the relatively large energy loss of the recoiling protons and alpha particles have longer decay times (100s to 1000s of ns). PSD and thus incident parti-

cle identification may be performed by recording the time dependence of the scintillation pulse form and comparing the fast and slow components.

2. ^{4}He as a scintillation medium for fast neutron detection

The development of both liquid and gaseous ^{4}He based scintillators for fast-neutron detection has been reported [6, 8, 12, 14, 15]. ^{4}He, like most noble gases, is a good scintillator. It has an ultra-violet light yield comparable to the intrinsic non-Tl doped light yield of NaI crystals [16–19]. Neutron interactions lead to ^{4}He recoils, where energy is deposited very locally within the gas. Gamma-ray interactions lead to recoiling electrons, which deposit only tens of keV per centimeter of trajectory. This difference in deposition density and therefore ionization density is believed to ultimately enable the PSD capability. PSD properties may be degraded significantly if the geometry and size of the detector results in a smearing of the transit times of scintillation photons comparible to the scintillation decay times. Good PSD also requires good scintillation efficiency; that is, a sufficient number of scintillation photons to define the time dependence of the pulse accurately, and low noise in the pulse-processing electronics.

With only two electrons per atom, ^{4}He has a very low charge density, thereby significantly limiting its sensitivity to gamma-rays. This is useful for fast-neutron detection, where insufficient gamma-ray rejection is often the factor which constrains the desired performance. The following physical effects contribute positively to the gamma-ray rejection performance of pressurized ^{4}He gas:

1. *Low gamma-ray interaction probability.* Due to the low electron density of ^{4}He, gamma-ray interaction probabilities are two orders of magnitude lower than neutron interaction probabilities.
2. *Low energy deposition.* Depending on the chosen geometry (i.e. a tube with radius of a few cm), the amount of energy the gamma-rays can deposit in the detector volume is limited. This is because the corresponding

Compton or pair electrons cannot transfer much energy to the gas before striking a detector wall.

3. *Similar scintillation-light yield for gamma-rays and neutrons.* The scintillation light production in organic liquid scintillators is highly velocity dependent. Thus, for the same amount of deposited energy, gamma-ray interactions produce more scintillation light than neutron interactions. In contrast, the scintillation-light yield for gamma-rays and neutrons is similar in noble-gas scintillators [17] such as ^{4}He. ^{4}He is commonly called a linear scintillator.
4. *PSD.* 1–3 above together with the fast and slow components of the ^{4}He scintillation signals lead to excellent PSD and thus excellent separation of neutrons and gamma-rays.

The purpose of this project was to compare the neutron/gamma discrimination obtained using the Arktis ^{4}He-based neutron-diagnostic tool (NDT) to that obtained using a reference liquid-scintillator cell filled with the organic liquid scintillator NE-213 [20].

3. Apparatus

3.1. Am/Be source

The detector characterizations reported on in this paper were carried out using a nominal 18.5 GBq ^{241}Am/^{9}Be (Am/Be) source [21] which emitted $(1.106\pm0.015) \times 10^6$ neutrons per second nearly isotropically [22]. The source is a mixture of americium oxide and beryllium metal contained in an X.3 capsule, which is a stainless-steel cylinder 31 mm (height) × 22.4 mm (diameter) [23]. ^{241}Am has a half-life of 432.2 years and decays via alpha-emission (5 discrete energies with an average value of about 5.5 MeV) to ^{237}Np. The dominant energy of the gamma-rays associated with the decay of the intermediate excited states in ^{237}Np is ∼60 keV. A 3 mm thick Pb sheet was used to complement the stainless steel X.3 capsule to attenuate these 60 keV gamma-rays. The half-value layer for 60 keV (1 MeV) gamma-rays for Pb is 0.12 mm (8 mm).

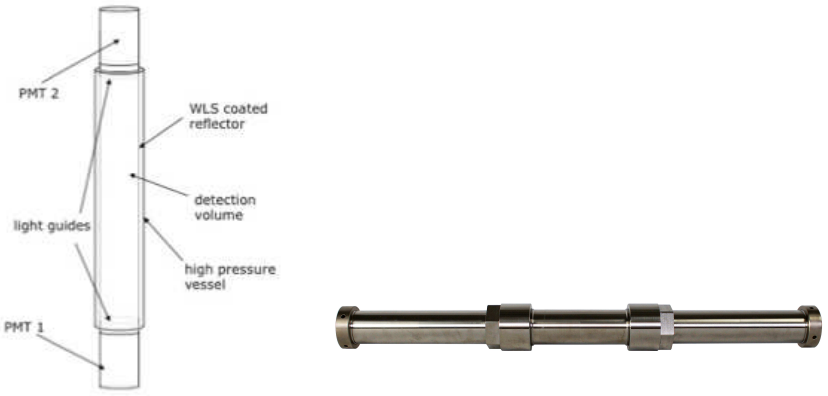

Figure 1: Schematic (left) and photograph (right) of the pressurized ^{4}He gas fast-neutron detector. The outer diameter was 5.08 cm (2") and the active length was 19.5 cm.

Neutrons are produced when the emitted alpha particles undergo a nuclear reaction with ^{9}Be resulting in ^{12}C and a free neutron. The resulting neutron distribution has a maximum energy of about 11 MeV [24], while approximately 25% of the neutrons have an energy of less than 1 MeV [25]. The de-excitation of the ^{12}C results in a 4.44 MeV gamma-ray about 55% of the time [25–27]. This gamma-ray is too energetic to be absorbed by the stainless steel of the X.3 capsule. Thus the radiation field from the Am/Be is a combination of high-energy gamma-rays and fast neutrons. Both the gamma-ray and fast-neutron dose rates at a distance of 1 m from the source in the unshielded X.3 capsule were measured using a Thermo Scientific Corporation FHT 752 dosimetric neutron detector [28]. They were both determined to be 11 μSv/hr for a total unshielded dose rate of 22 μSv/hr, in exact agreement with the data sheet from the supplier.

3.2. Arktis pressurized ^{4}He gas Neutron Diagnostic Tool (NDT)

The version of the Arktis pressurized gas ^{4}He fast NDT used for these measurements is shown in Fig. 1. It was of cylindrical geometry with an outer diameter of 5.08 cm (2") and a 19.5 cm active length. The detector walls were

made of stainless steel. The interior surface of the stainless-steel cylinder was coated with a PTFE-based diffuse reflector [29] which was itself coated with an organic phosphor that converted the wavelength of the scintillation light from 80 nm to 430 nm. As ^{4}He is transparent to its own light, almost no signal loss due to reabsorption occurs [30]. The predominant mechanism for signal loss was due to multiple reflections inside the detector. Optical windows capable of withstanding the 120 bar operating pressure were employed. The scintillation signals were read out at both ends of the active volume by Hamamatsu R580 [31] photomultiplier tubes (PMTs).

3.3. NE-213 reference detector

The NE-213 reference detector is shown in Fig. 2. The core of the NE-213 reference detector was a 3 mm thick cylindrical aluminum cell with an inner depth of 62 mm and an inner diameter of 94 mm. The inside of the cell was painted with EJ-520 [32] titanium dioxide reflective paint, which can withstand the xylene solvent of the liquid scintillator. The aluminum cell was sealed using a 5 mm thick borosilicate glass window [33] glued to the aluminum cell using the highly temperature and chemical resistant Araldite 2000+ [34]. The 2 penetrations into the cell which allowed for filling were sealed with M-8 threaded aluminum plugs with 20 mm diameter heads and 14 mm diameter Viton O-rings [35]. Nitrogen gas was bubbled through the NE-213 liquid scintillator for 24 hours prior to filling the cell. The assembled cell was then filled with the nitrogen-flushed NE-213 using a nitrogen gas transfer system.

After filling, the borosilicate glass window of the cell was coupled to a cylindrical PMMA [36] lightguide with a depth of 57 mm and a diameter of 72.5 mm. PMMA is an acrylic which transmits light down to 300 nm in wavelength [37]. The cylindrical surface of this lightguide was painted with water-soluble EJ-510 [38] reflective paint. The lightguide was then pressure-coupled via springs to a magnetically shielded 3 inch ET Enterprises 9821KB PMT assembly [39]. No optical-coupling grease was used.

Figure 2: The NE-213 reference detector. Top: a detail of the cylinder "cup". The screws on top allow for the filling or draining of the liquid cylinder. A borosilicate-glass window (light brown) serves as the optical boundary. See text for details. Bottom: The black cylinder to the right is the magnetically shielded 3 inch ET Enterprises 9821KB photomultiplier-tube assembly. The gray cylinder to the left is the "cup". (For interpretation of the references to color in this figure caption, the reader is referred to the web version of this article.)

3.4. Arktis WaveDREAM-B16 digitizer

The analog signals from the NDT and NE-213 reference cell were fed directly to a WaveDREAM-B16 high-precision digitizer developed by Arktis Radiation Detectors [40] (see Fig. 3). After being converted to a digital signal, the data of interest were stored for analysis. The decision for storage was based on a 120 megasample per second (MSPS) signal that was continuously read out and fed into a field programmable gate array (FPGA). If the user-defined trigger condition was met (see below for the trigger conditions employed in this measurement), the FPGA read out the DRS4 switched capacitor array [41] containing the stored waveform at 1 gigasample per second (GSPS). Complete details are presented in Ref. [42]. In this manner, excellent time resolution (provided by the 1 GSPS sampling and nanosecond time stamping also between different detectors) was achieved at 10-bit resolution over the 3.5 μs duration of the stored event. The trigger conditions were user-configurable. In the case of the

NDT, a trigger occurred only if the signals from both PMTs mounted on each end of the detector were above threshold. This threshold was 35 scintillation photons detected above the ambient baseline, and suppressed the dark-current count rate. An event was considered to be valid if the second PMT signal came less than 32 ns after the first, a criterion related to the dimensions of the ^{4}He gas volume and the speed of light. In the case of the NE-213 reference cell which had only one PMT, a trigger occurred if the analog signal coming from the PMT was above threshold. This threshold was 30 scintillation photons detected above the ambient baseline. The digitizer greatly facilitated the offline analysis of the data as it allowed for the Arktis NDT PMTs to be synchronized to better than 1 ns. It also allowed for offline variation in the detector thresholds and integration gates (see below), a clear advantage over standard discriminators and analog-to-digital converters.

4. Measurement

4.1. Setup

The experiment setup is shown in Fig. 5. The Am/Be source in its transport/storage container was placed at the center of a 4-sided enclosure constructed from borated-wax boxes. In the so-called "park" position with the source locked in its transport container at the bottom of the borated-wax box enclosure, the total dose rate in the room was less than 0.4 μSv/hr. When the source was lifted from its container and positioned within the 3 mm Pb thick sleeve, the gamma-ray dose rate on the outside of the 4-sided borated-wax enclosure was 1 μSv/hr.

Square penetrations through 2 of the opposite walls of the enclosure allowed direct line-of-sight between the detectors being irradiated and the source. A HPGe gamma-ray detector was positioned in one of the apertures. The distance to the screened source was $\sim$1 m and line-of-sight was direct. It was used to measure the distribution of gamma-rays at the approximate location of the NDT and NE-213 reference cell. Fig. 4 presents this distribution, where the

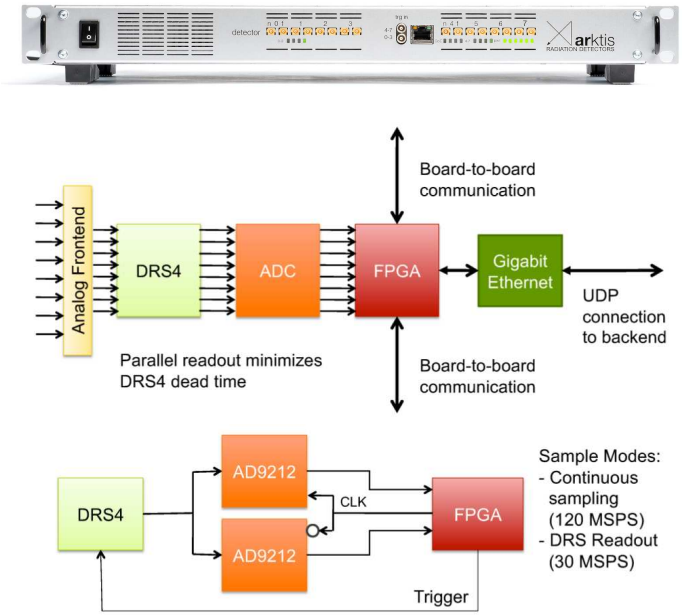

Figure 3: The top figure shows the WaveDREAM-B16. There are 16 input channels grouped in 2 clusters of 8. Once the selected signals are digitized, they are read out via Gigabit ethernet. Triggers can be applied externally or generated internally by the software. The middle figure is a schematic overview of the readout electronics. Signals are stored in the DRS4 switched-capacitor array and read out if user-defined trigger conditions are met. The bottom figure presents an overview of the software trigger. If the signal sampled at 120 MSPS meets the trigger condition, the FPGA reads out the DRS4 at 1 GSPS. See Ref. [42] for further details.

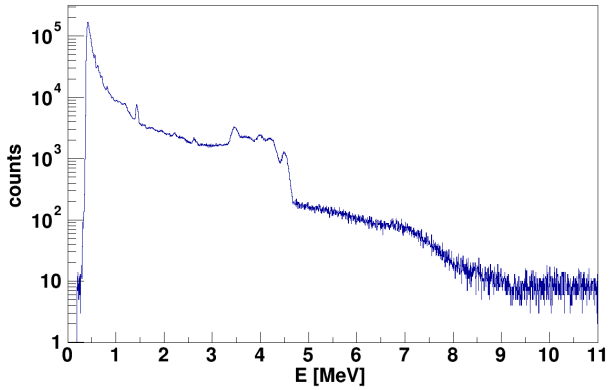

Figure 4: Energy distribution of gamma-rays at the approximate location of the NDT and NE-213 reference cell. The prominent structure between 3 and 5 MeV results from the 4.44 MeV gamma-ray.

4.44 MeV gamma-ray peak together with its Compton edge, first- and second-escape peaks, and their Compton edges are clearly seen between (from the right) 5 and 3 MeV. Between 1.0 MeV and the ∼400 keV detector threshold, the gamma-ray intensity increased by an order-of-magnitude.

At a distance of 0.64 m from the source, the square aperture for the NE-213 reference detector was 17×17 cm^2. The cell was placed at source height so that the face of the active volume (recall Fig. 2) was 70 cm from the center of the Am/Be source. The cylindrical symmetry axis of the detector pointed directly at the center of the source. It was operated at -1700 V. The analog signals from the single PMT were fed into the digitizer. The digitized waveforms of the signals which triggered the acquisition were recorded on an event-by-event basis for offline processing. At the same distance from the source, the square aperture for the NDT was 25×25 cm^2. The NDT was also placed at source height. However, its cylindrical symmetry axis was perpendicular to the ray pointing to the center of the source. Both of the PMTs (one at each end of the detector volume) were operated at +1730 V. The analog signals from these PMTs were fed into the digitizer. Again, the digitized waveforms of the signals

which triggered the acquisition were recorded on an event-by-event basis for offline processing.

A pulse-shape (PS) analysis of the analog signals coming from both detectors was performed using the "tail-to-total" method. Two integration gates were defined, a long gate (LG) and a short gate (SG). Both of the gates opened at the same time, 10 ns before the analog signal. The SG was used to integrate only the fast components of the analog signal, while the LG was used to integrate the entire (both fast and slow components) analog signal. The PS was determined from the difference between the scintillation-light yield in the LG and SG normalized to the scintillation-light yield in the LG: PS = (LG-SG)/LG. For the NDT PMT data, the SG was 100 ns (related to the decay constant of the fast-scintillation components of ^{4}He) and the LG was 3500 ns (the maximum gate length the digitizer provided). For the NE-213 reference cell data, the SG was 25 ns and the LG was 150 ns. The Arktis NDT gate widths were optimized offline. This procedure was greatly facilitated by the digitizer.

4.2. Absolute energy calibration

Energy-calibration measurements for the NE-213 reference cell were performed using ^{60}Co, ^{137}Cs, and the Pb-shielded Am/Be sources. ^{60}Co emits gamma-rays with energies 1.17 MeV and 1.33 MeV. ^{137}Cs emits a gamma-ray with an energy 0.66 MeV. The de-excitation gamma-ray from the first excited state of ^{12}C has an energy of 4.44 MeV. The locations of the Compton edges from these gamma-rays were determined using the prescription of Knox and Miller [43].

For the NDT, Geant4 simulations [44, 45] reproduce the shape of the observed pulse-height distributions for neutrons and gamma-rays well. Neutrons, which produce a recoiling α particle, were correlated directly to the 5.5, 6.0, and 7.7 MeV α lines in ^{222}Rn [8]. Gamma-rays produce an electron via Compton scattering or an electron and positron via pair production. These interactions occur dominantly in the relatively high-Z walls of the NDT. Apart from very low energies, most electrons or positrons entering the ^{4}He gas volume do not

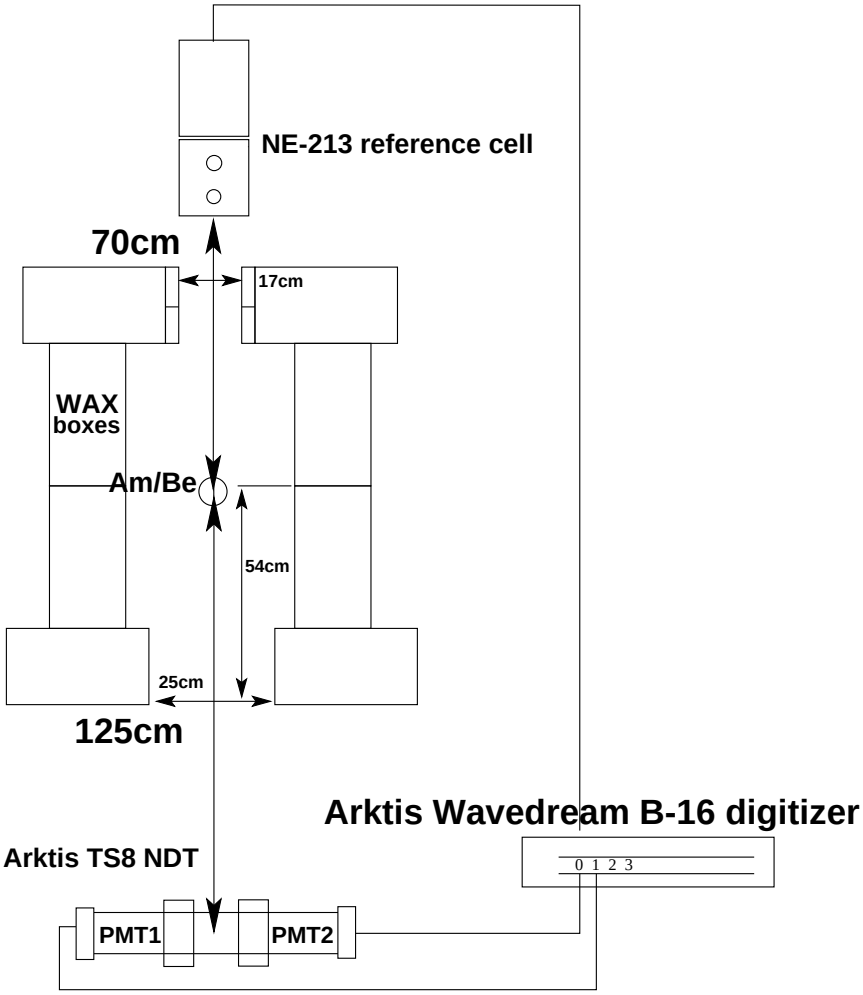

Figure 5: The experiment setup (not to scale). The Am/Be source was placed at the center of a borated-wax enclosure. Penetrations through two of the enclosure walls allowed for a direct line-of-sight between the source and the detectors. For measurements of the gamma-ray distribution at the apertures, the NE-213 reference cell was replaced with a stand-alone HPGe detector.

stop in the gas. On traversing the gas, they loose a fairly well-defined energy of around 150 keV. This produces a peak in the pulse-height distribution which can be used for cross calibration. The energy-loss distribution extends out to around 750 keV, which is more or less independent of the incident gamma-ray energies above 750 keV. These energy losses are of course dependent upon the size and pressure of the ^{4}He gas volume. From this, we have established that the scintillation-light yield is the same for electrons and alpha particles, consistent with ^{4}He being a linear scintillator. This contrasts with NE-213, where the scintillation-light yield depends strongly on the velocity and ionization density of the interacting particle.

5. Results

Figure 6 shows a two-dimensional scatterplot comparison of the PSD achieved using the NE-213 reference cell and the ^{4}He-based NDT obtained using the Pb-screened Am/Be source. Recall that the Pb-screened Am/Be source provided a continuous energy spectrum of neutrons up to 11 MeV and a of gamma-rays up to 4.44 MeV. The gamma-ray pulse-height response of the NE-213 reference cell extends to 4 MeV$_{ee}$ as shown in the upper panel. Below 500 keV$_{ee}$, significant overlap between the neutron and gamma-ray pulse-height responses occurred. As shown in the lower panel and in stark contrast, the gamma-ray pulse-height response of the Arktis NDT extends only to 750 keV$_{ee}$, and clear separation between the neutron and gamma-ray pulse-height responses is evident down to 100 keV$_{ee}$.

The amount of scintillation light produced in the gaseous ^{4}He is less than that produced in the liquid scintillator for both particle types. In absolute terms, the detection efficiency of the NE-213 reference cell will qualitatively be higher the Arktis NDT, both for neutrons and gamma-rays. Quantitative evaluation of these detection efficiencies and comparisons with Monte Carlo calculations will be addressed in a future publication. We note that the lower absolute detection efficiency of the Arktis NDT could be advantageous in very

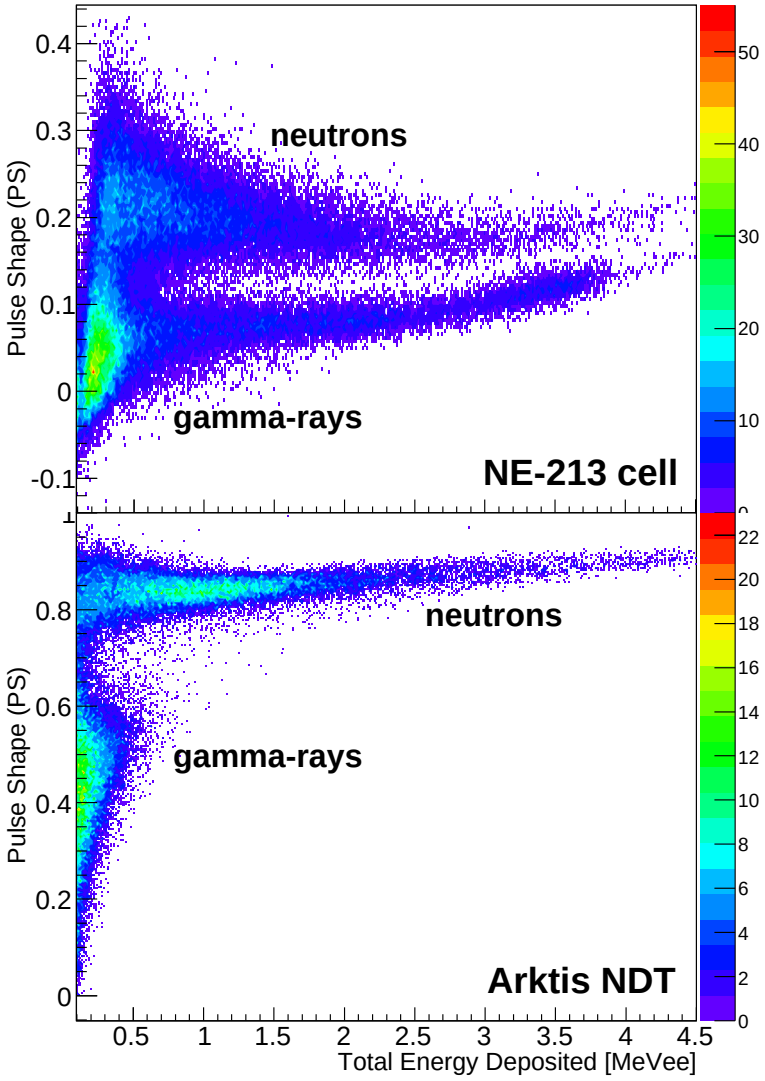

Figure 6: A comparison of the PSD achieved using the NE-213 reference cell (top panel) and the ^{4}He-based NDT (bottom panel) with the Pb-screened Am/Be source. For each event, the signal pulse shape PS = (LG-SG)/LG has been plotted against the scintillation-light yield produced in the detector for the LG in MeV$_{ee}$. The distributions corresponding to neutrons and gamma-rays are labeled.

high intensity radiation fields. The complete lack of a gamma-ray band to higher energies in the bottom scatterplot is striking. Relative to the numbers of neutrons detected, the gamma-ray discrimination properties of the Arktis NDT are clearly superior. The digitizer clearly proved to be a very effective tool for optimizing the PSD.

One-dimensional projections of PS have been obtained from the two-dimensional distributions shown in Fig. 6 for five different pulse-height thresholds. The resulting PS distributions for the NE-213 detector (left column) and Arktis NDT (right column) integrated from these thresholds are shown in Fig. 7. In each of the panels, wherever possible, two separate Gaussian functions have been fitted to the data – one corresponding to gamma-rays (red) and one corresponding to neutrons (blue). A standard figure-of-merit (FOM) has been used to quantify the quality of the PSD as a function of deposited-energy cut. This FOM is given by the separation between the gamma-ray and neutron peaks divided by the sum of the FWHM of these peaks.

As can be seen in the NE-213 data (left column), the FOM improves from 0.75 to 1.5 as the requirement on the light yield increases from 0.25 to 3.0 MeV_{ee}. In comparison, the Arktis NDT FOM (right column) improves from 1.35 to 1.70 as the requirement on the light yield increases from 0.25 to 0.50 MeV_{ee}. Once the requirement on the amount of deposited energy exceeds 0.75 MeV_{ee}, the gamma-ray peak is no longer visible in the Arktis NDT, and the signal is unambiguously neutron. Again, the fact that gamma-rays with energies up to 4.44 MeV deposit no more than 750 keV_{ee} in the Arktis NDT is striking. This property of the detector greatly facilitates the identification of fast neutrons depositing more energy than this value.

6. Summary

A first comparison between the PSD characteristics of a novel ^{4}He-based high-pressure gas scintillation detector and a standard NE-213 liquid-scintillator reference detector has been performed. A Pb-screened Am/Be mixed-field neu-

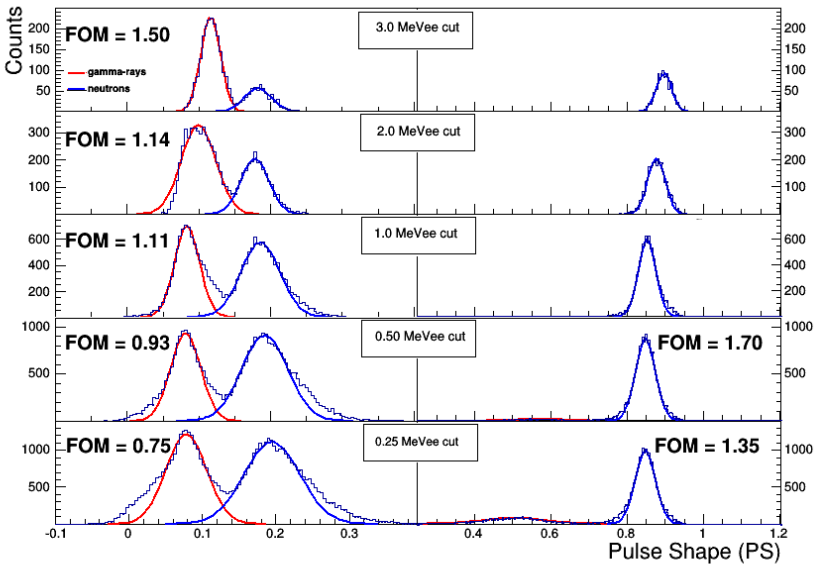

Figure 7: A first comparison of the PSD achieved using the NE-213 reference cell (left column) and the ^{4}He-based NDT (right column) via a FOM using the Pb-screened Am/Be source and varying the requirements on the amount of energy deposited in the detectors. Gamma-rays with energies up to 4.44 MeV deposit no more than 750 keV$_{ee}$ in the Arktis NDT which greatly facilitates fast-neutron particle identification.

tron and gamma-ray source was used to irradiate the detectors and a high-resolution scintillation-pulse digitizer was used to optimize the PSD using the tail-to-total method. The NE-213 liquid-scintillator reference cell was differentially very sensitive to the incident gamma-rays and registered a wide range of scintillation-light yields up to 4.4 MeV_{ee}. In contrast, the ^{4}He-based NDT was designed to have has a low gamma-ray sensitivity. It registered a maximum scintillation-light yield of 750 keV_{ee} for the same distribution of incoming gamma-rays. The PSD obtained with the NE-213 liquid-scintillator reference cell, facilitated by using the digitizer, was good. Clear separation between neutrons and gamma-rays was obtained down to about 0.5 MeV_{ee}. The PSD obtained with the ^{4}He-based NDT was excellent. Clear separation between neutrons and gamma-rays was obtained down to 0.1 MeV_{ee}. Most striking was the fact that gamma-rays of energies up to 4.44 MeV resulted in scintillation-light yields of no more than 750 keV_{ee} in the NDT. As a result, a simple threshold cut above 750 keV_{ee} was sufficient to distinguish fast neutrons from gamma-rays in this region. For fast-neutron detection, ^{4}He-based high-pressure gas scintillation detectors such as the NDT thus have a clear advantage over liquid-scintillator detectors such as the NE-213 reference cell when the scintillation-light yield is greater than 750 keV_{ee}.

The next step in our investigations shall involve an expanded systematic comparison of the PSD obtained with these two scintillators using a FOM as a function of scintillation-light yield. The scintillation-light yield as a function of neutron energy must also be established if the potential for spectroscopy is to be investigated. In order to perform these investigations, knowledge of the incident neutron energies is required. We have recently successfully tested a technique for performing such irradiations with Be-compound neutron sources [46] which relies on well-understood shielding, coincidence, and time-of-flight measurement techniques to produce a polychromatic energy-tagged neutron beam.

Acknowledgements

We thank the Photonuclear Group at the MAX IV Laboratory for providing access to their experimental hall and Am/Be source. We acknowledge the support of the UK Science and Technology Facilities Council (Grant nos. STFC 57071/1 and STFC 50727/1).

References

[1] Uses of neutrons in engineering and technology, J. Walker, Phys. Technol. 13 (1982) 239, doi: 10.1088/0305-4624/13/6/I01.

[2] United States Committee on Army Science and Technology for Homeland Defense, Board on Army Science and Technology, Division on Engineering and Physical Sciences, National Research Council, Indications and Warning Technologies, in Science and Technology for Army Homeland Security: Report 1, National Academies Press (2003), ISBN: 9780309087018, http://www.nap.edu/openbook.php?record_id=10655.

[3] International Workshop on Fast Neutron Detectors and Applications (FNDA2006), University of Capetown, South Africa (2006), Proceedings of Science (FNDA2006). http://pos.sissa.it/cgi-bin/reader/conf.cgi?confid=25.

[4] 2nd International Workshop on Fast Neutron Detectors and Applications (FNDA2011), Kibbutz Ein Gedi, Israel (2011), JINST 7 C (2012). http://iopscience.iop.org/1748-0221/focus/extra.proc19.

[5] Proceedings from the workshop on Neutron, Neutrino, Nuclear, Muon and Medical Physics at ESS, Lund, Sweden (2009). http://www.hep.lu.se/staff/christiansen/proceeding.pdf.

[6] Fast neutron detection in homeland security applications, R. Chandra, G. Davatz, U. Gendotti, A. Howard, IEEE NSS/MIC (2010) 508, doi: 10.1109/NSSMIC.2010.5873813.

[7] Drilling and Well Completions, Reservoir Engineering, in Standard Handbook of Petroleum and Natural Gas Engineering, 2nd edition, W.C. Lyons, G.J. Plisga, Elsevier Science (2011), ISBN: 978-0-7506-7785-1.

[8] Fast neutron detection with pressurized ^{4}He scintillation detectors, R. Chandra, G. Davatz, H. Friederich, U. Gendotti, D. Murer, JINST 7.03 (2012) C03035, doi: 10.1088/1748-0221/7/03/C03035.

[9] Testing on novel neutron detectors as alternative to ^{3}He for security applications, P. Peerani, A. Tomanin, S. Pozzi, J. Dolan, E. Miller, M. Flaska, M. Battaglieri, R. De Vita, L. Ficini, G. Ottonello, G. Ricco, G. Dermody, C. Giles, Nucl. Instr. and Meth. in Phys. Res. A 696 (2012) 110, doi: 10.1016/j.nima.2012.07.025.

[10] Workshop on fast neutron applications at spallation sources, Abingdon, UK (2013). http://plone.esss.lu.se/.

[11] Current Practice in Well Logging, Reservoir Engineering and Secondary Recovery, in The Petroleum Engineering Handbook: Sustainable Operations, M.R. Islam, M.I. Khan, Elsevier Science (2013), ISBN: 9780127999838, http://books.google.com/books?id=xXijAQAAQBAJ.

[12] Analysis for In-situ Fission Rate Measurements using 4He Gas Scintillation Detectors, 3rd International Conference on Advancements in Nuclear Instrumenation Measurement Methods and their Applications, J.L. Lewis, D. Raetz, D. Murer, K.A. Jordan, Marseille, France (2013), doi: 10.1109/ANIMMA.2013.6728031.

[13] Characterization of a cubic EJ-309 liquid scintillator detector, A. Tomanin, J. Paepen, P. Schillebeeckx, R. Wynants, R. Nolte, A. Lavietes, Nucl. Instr. and Meth. in Phys. Res. A 756 (2014) 45, doi: 10.1016/j.nima.2014.03.028.

[14] Fission signal detection using helium-4 gas fast neutron scintillation detectors, J.M. Lewis, R.P. Kelley, D. Murer, K.A. Jordan, Appl. Phys. Lett. 105 (2014) 014102, doi: 10.1063/1.4887366.

[15] Time dependence of liquid-helium fluorescence, D.N. McKinsey, C.R. Brome, S.N. Dzhosyuk, R. Golub, K. Habicht, P.R. Huffman, E. Korobkina, S.K. Lamoreaux, C.E.H. Mattoni, A.K. Thompson, L. Yang, J.M. Doyle, Phys. Rev. A 67 (2003) 062716, doi: 10.1103/PhysRevA.67.062716.

[16] Scintillation detectors, in Noble gas detectors, E. Aprile, A.E. Bolotnikov, A.I. Bolozdynya, T. Doke, Wiley-VCH Verlag GmbH, KGaA, Weinheim Germany (2006), ISBN: 978-3-527-40597-8

[17] The theory and practice of scintillation counting, J.B. Birks, D.W. Fry, L. Costrell, K. Kandish, Pergamon Press, New York, U.S.A. (1964), ISBN: 978-0-08-010472-0.

[18] Radiation detection and measurement, G.F. Knoll, Wiley, New York, U.S.A. (1989), ISBN: 9780471815044, http://books.google.com/books?id=dyBRAAAAMAAJ.

[19] The mechanism of noble gas scintillation, in Elementary particles and cosmic rays, B.A. Dolgosheim, B.U. Rodionov, Volume 2, Atomizdat, Moscow Russia (1969).

[20] NE213 is no longer produced. Eljen Technologies offers EJ-301 (http://www.eljentechnology.com/index.php/products/liquid-scintillators/71-ej-301) while Saint Gobain offers BC-501 (http://www.detectors.saint-gobain.com/uploadedFiles/SGdetectors/Documents/Product_Data_Sheets/BC501-501A-519-Data-Sheet.pdf).

[21] supplied by High Tech Sources Limited, Unit 6, Moorbrook, Southmead, Industrial Estate, Didcot, Oxfordshire, UK OX11 7HP; https://www.hightechsource.co.uk.

[22] testing performed at National Physical Laobratory, Teddington, Middlesex, UK TW11 0LW on 24 January 2012.

[23] http://www.hightechsource.co.uk/Legacy/Resources/Americium-Beryllium.pdf for details.

[24] Neutron Spectra of ^{214}Am/B, ^{241}Am/Be, ^{241}Am/F, ^{242}Cm/Be, ^{238}Pu/^{13}C and ^{252}Cf isotopic neutron sources, E.A. Lorch, Int. J. Appl. Radiat. Is. 24 (1973) 585, doi: 10.1016/0020-708X(73)90127-0.

[25] The neutron spectrum of Am-Be neutron sources, A.D. Vijaya, A. Kumar, Nucl. Instrum. and Meth. 111 (1973) 435, doi: 10.1016/0029-554X(73)90199-7.

[26] Determination of 4.438 MeV γ-ray to neutron emission ratio from a ^{241}Am-^{9}Be neutron source, A.A Mowlavi, R. Koohi-Fayegh, Appl. Radiat. Isot. 60 (2004) 959, doi: 10.1016/j.apradiso.2004.02.008.

[27] The 4.438 MeV gamma to neutron ratio for the AmBe neutron source, Zhenzhou Liu, Jinxiang Chen, Pei Zhu, Yongming Li, Guohui Zhang, Appl. Radiat. Isot. 65 (2007) 1318, doi: 10.1016/j.apradiso.2007.04.007.

[28] http://www.laurussystems.com/products/products_pdf/LS_thermo_FH-40.pdf

[29] Polytetrafluoroethylene, also known as Teflon. http://www2.dupont.com/Teflon_Industrial/en_US/products/selection_guides/coatings.html.

[30] D.N. McKinsey, C.R. Bromea, J.S. Butterworth, S.N. Dzhosyuk, R. Golub, K. Habicht, P.R. Huffman, C.E.H. Mattoni, L. Yang, J.M. Doyle Detecting ionizing radiation in liquid helium using wavelength shifting light collection, Nuc. Instr. Meth. 516, Issue 2-3, p. 475-485.

[31] http://www.hamamatsu.com/us/en/R580.html

[32] http://www.eljentechnology.com/index.php/products/paints/87-ej-520.

[33] http://www.us.schott.com/borofloat/english/index.html for details. Supplied by Glasteknik i Emmaboda AB, Utvägen 6 SE-361 31 Emmaboda, Sweden.

[34] Araldite is a registered trademark of Huntsman. See http://www.araldite2000plus.com.

[35] Viton is a registered trademark of DuPont Performance Elastomers LLC.

[36] Poly(methyl-methacrylate), also known as acrylic, plexiglass, and lucite. Supplied by Nordic Plastics Group AB, Bronsyxegatan 6, SE-213 75 Malmö, Sweden.

[37] http://www.eljentechnology.com/index.php/products/pmma-a-uvt-material/102-light-guides

[38] http://www.eljentechnology.com/index.php/products/paints/86-ej-510.

[39] http://www.et-enterprises.com/files/file/Pmtbrochure11.pdf for details.

[40] Arktis Radiation Detectors Limited, 8045 Zürich, Switzerland; http://www.arktis-detectors.com.

[41] S. Ritt, Design and Performance of the 6 GHz Waveform Digitizing Chip DRS4, in IEEE Nuclear Science Symposium Conference, NSS 08, Oct 2008, pp. 1512-1515.

[42] A Scalable DAQ System Based on the DRS4 Waveform Digitizing Chip, H. Friederich, G. Davatz, U. Hartmann, A. Howard, H. Meyer, D. Murer, S. Ritt, N. Schlumpf, IEEE Trans. Nucl. Sci. 58 (2011) 1652, doi: 10.1109/TNS.2011.2159623.

[43] A technique for determining bias settings for organic scintillators, H.H. Knox, T.G. Miller, Nucl. Instrum. and Meth. 101 (1972) 519, doi: 10.1016/0029-554X(72)90040-7.

[44] S. Agostinelli et al., Geant 4: A Simulation toolkit, Nucl. Instrum. Meth. A 506 (2003) 250, doi: 10.1016/S0168-9002(03)01368-8.

[45] J. Allison et al., Geant4 developments and applications, IEEE Trans. Nucl. Sci. 53 (2006) 270, doi: 10.1109/TNS.2006.869826.

[46] Tagging fast neutrons from an $^{241}Am/^{9}Be$ source, J. Scherzinger, J.R.M. Annand, G. Davatz, K.G. Fissum, U. Gendotti, R. Hall-Wilton, E. Håkansson, R. Jebali, K. Kanaki, M. Lundin, B. Nilsson, A. Rosborg, H. Svensson, Applied Radiation and Isotopes 98 (2015) 74, doi: 10.1016/j.apradiso.2015.01.003.

PAPER III

An in-depth characterization of a NE-213 reference detector with a tagged neutron source

J. Scherzinger[a,b,*], K.G. Fissum[a,b], J.R.M. Annand[c], R. Hall-Wilton[b,d], A. Hansson[e], E. Håkansson[a], R. Jebali[f,1], K. Kanaki[b], M. Lundin[e], B. Nilsson[b,e], H. Sevensson[e]

[a] *Division of Nuclear Physics, Lund University, SE-221 00 Lund, Sweden*
[b] *Detector Group, European Spallation Source ESS AB, SE-221 00 Lund, Sweden*
[c] *University of Glasgow, Glasgow G12 8QQ, Scotland, UK*
[d] *Mid-Sweden University, SE-851 70 Sundsvall, Sweden*
[e] *MAX IV Laboratory, Lund University, SE221 00 Lund, Sweden*
[f] *Arktis Radiation Detectors Limited, 8045 Zürich, Switzerland*
[g] *Your address*

Abstract

We report on an in depth characterization of a NE-213 liquid scintillator detector with a tagged neutron source for fast neutrons between 2 MeV and 7 MeV. The excellent pulse-shape discrimination of the scintillator and a time-of-flight measurement have been employed to establish a proton light yield function in electron equivalent energies. The here established proton light yield function agrees well with the measurements of other groups.

Keywords: light yield, pulse-shape discrimination, tagged neutrons

1. Introduction

Fast-neutrons are used in a wide range of experiments in nuclear physics and beyond [1, 2, 3, 4, 5, 6, 7]. New detector systems to study fast-neutrons has to be thoroughly tested before they can be deployed. Standard test probes are quasi-mono-energetic neutron beams, produced with accelerators [8, 9, 10]. The cost per neutron from such beams is high. A cost efficient alternative is the use of radioactive neutron sources [11, 12]. We are developing such a source

*Corresponding author. Telephon: +46 46 222 7733; Fax: + 46 46 222 9677
Email address: julius.scherzinger@nuclear.lu.se (J. Scherzinger)
[1] present address: University of Glasgow, Glasgow G12 8QQ, Scotland, UK

based facility for energies between 2 - 6 MeV by using tagged neutrons to from a poly-chromatic neutron beam [13]. We demonstrate the working principle by an in-depth analysis of the commonly used liquid scintillator, NE-213 [14]. This organic solvent is regarded by many as the "gold standard" for the detection of fast neutrons. We were particular interested in two important characteristics of the liquid scintillator detector, the light yield of neutron induced recoiling protons and the Figures-of-Merit (FOM) at different light yields, numbers indicating the discrimination strength of the detector between neutrons and gammas. The here investigated detector will be used in the future as a fast neutron reference detector at the source facility.

2. Apparatus

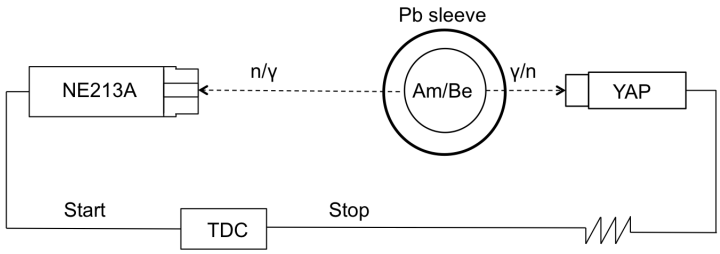

Figure 1: A not to scale block diagram of the experimental set-up. The Pb sleeve attenuates the 60 keV gammas from the source. The logic for the time-of-flight measurement is illustrated.

2.1. Americium Beryllium Neutron Source

An 18.5 GBq ^{241}Am/^{9}Be neutron source (hereafter referred to as AmBe) was used to irradiate a free running NE-213 detector and two free running Ytrrium-Aluminium-Pervoksit (YAP) coincidence detectors. The source is an mixture between americium oxide and beryllium metal, contained in an approximately 30 mm (height) x 22 mm (diameter) type X.3 stainless steel capsule [15] , and emits

$(1.106\pm0.015)\cdot10^6$ neutrons per second nearly isotropically. ^{241}Am has a half-life of 432.2 years and decays to ^{237}Np by alpha-emissions with an average energy of 5.5 MeV. The 60 keV gamma-rays from an intermediate excitation state of ^{237}Np are the dominating gamma radiation. The source creates fast neutrons primarily by a nuclear reaction between alpha particles and ^{9}Be resulting in a free neutron and ^{12}C. The neutrons have a maximum energy of about 11 MeV, while 25% are estimated to have an energy of less than 1 MeV. This yields an average neutron energy of roughly 4.5 MeV. The fast neutron is in $\sim$ 55% accompanied by a 4.43 MeV gamma-ray from the de-excitation of the first excited nuclear state of ^{12}C. These gamma-rays are to energetic to be absorbed in the stainless steel capsule. Thus the combination of both fast neutrons and MeV gamma-rays contributing to the AmBe dose rate. Both the fast neutron dose rate and the gamma-ray dose rate of the unshielded AmBe source have been measured independently at a distance of 1 m to the source to 11 μSv/hr respectively, yielding a total dose rate of 22 μSv/hr.

The NE-213 detector was used to trigger the data acquisition system and the signal was also used to start a time-to-digital convert (TDC). The TDC was stopped by delayed signals from either of the two YAPs. A neutron time-of-flight (ToF) measurement could be easily performed with this configuration.

2.2. YAP Trigger Detector

Two YAP:Ce3 scintillator detectors from Scionix [16] with $\sim$ 5 ns risetime were used as fast trigger detectors. A detector (see Fig. 2) consisted of a cylindrical (h = 2.54 cm x d = 2.54 cm) YAP crystal coupled to a 1 inch R1924 Hamamatsu PMT [17] operated at about -800 V. Gains for the YAP detectors were set using a YAP event trigger and standard gamma-ray sources. Typical energy resolution obtained for the 662 keV peak of ^{137}Cs using such a detector was about 10%. YAP crystals are radiation hard and quite insensitive to neutrons of all energies, which makes them ideal for detecting gamma-rays within the large fast-neutron field of the AmBe source. The YAP detectors were not used for spectroscopy, but triggered on any portion of the energy

Figure 2: Photo of a YAP trigger detector.

deposited by the 4.43 MeV gamma-rays. A 3 mm thick Pb sleeve placed around the source to attenuate the high intensity 60 keV gamma-ray field and a very low discriminator threshold proved to be an effective combination for the YAP detection of these 4.43 MeV gamma-rays.

2.3. NE-213 Fast-Neutron Detector

The fast-neutron detector is shown in Fig. 3. The NE-213 is housed in a 3 mm thick cylindrical aluminum cell with a diameter of 94 mm and a height of 62 mm. The inner walls of the cell were painted with EJ-520 [18], a xylene-solvent withstanding titanium-dioxide reflective paint. Araldite 2000+ [19] glue, which is highly resistant to both temperature and chemicals, sealed a 5 mm thick borosilicate glass plate [20] to the detector cell. The penetrations into the cell were closed with M-8 threaded aluminum plugs with 20 mm diameter heads and sealed with 14 mm diameter Viton O-rings [21]. The assembled cell was filled with the nitrogen-flushed NE-213 using a nitrogen gas-transfer system. The filled cell was optical coupled to a cylindrical ultraviolet transmitting polymethyl-methacrylate (PMMA UVT) lightguide [22] with a height of 57 mm and a diameter of 72.5 mm. The lightguide wall was painted with water-

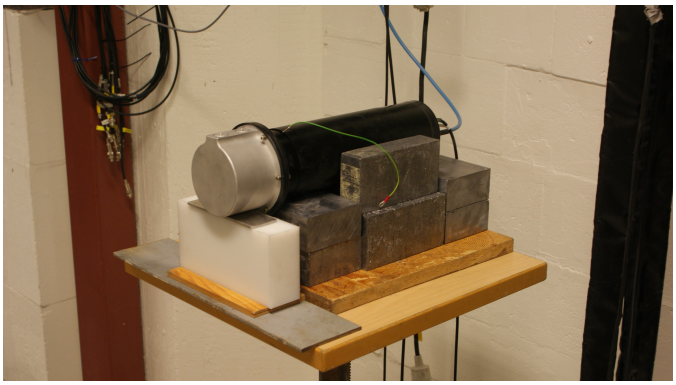

Figure 3: The liquid scintillator detector. The black cylinder covering the PMT housing is the Mu-metal shielding the 3 inch ET Enterprises 9821KB PMT from stray magnetic fields. The metallic cylindrical capsule at the front of the detector contains the NE-213.

soluble EJ-510 [23] reflective paint. The lightguide was then pressure-coupled to a spring-loaded, magnetically shielded 3 inch ET Enterprises 9821KB PMT assembly [24] operated at about 2000 V. The gain for the NE-213 detector was set using an NE-213 detector event trigger and a set of standard gamma-ray sources together with the prescription of Knox and Miller [25].

2.4. Experimental Set-Up

Figure 1 illustrated the experimental set-up in a block diagram. The AmBe source was placed in a 3 mm thick lead cylinder to attenuate the low energy gamma field ($\sim$ 60keV) from the decay of ^{241}Am. The YAP detectors were placed 5 cm from the source in the same height as the source. The YAP detectors were free running and registered mainly the the 4.43 MeV gamma-rays from the source. The NE-213 detector was positioned 0.68 m from the source in direct line of sight. The cylindrical symmetry axis of the detector was centered to the source. The NE-213 detector was free running and triggered on the gamma-rays and neutrons from the source, as well as the natural background.

2.5. Data Acquisition

The signals from the YAP trigger detectors and the NE-213 detector were passed to scalers, time-to-digital converters (TDCs), and charge-to-digital converters (QDCs). All signals were stored in an event-by-event basis and processed offline. In calibration mode, the YAP detector trigger was used to gate the YAP detector QDC, to set the gain . In time-of-flight mode, the NE-213 detector provided the trigger which was used to gate the NE-213 detector QDCs (which facilitated setting the gain). The NE-213 detector QDCs included a short-gated (SG) QDC and a long-gated (LG) QDC, both of which opened 25 ns before the analog pulse arrived. The NE-213 detector also provided the start trigger for the time-of-flight TDC (see Fig. 1), while the YAP trigger provided the stop trigger. By triggering our data-acquisition system on the NE-213 detector, we avoided unnecessary deadtime processing events seen only by the YAPs and guarantied that the NE-213 pulses arrived 25 ns after the QDC gates were opened. We were especially interested in tow different time-correlated coincidences; the first, fast neutrons detected in the NE-213 detector starting the time-of-flight TDC with the corresponding 4.43 MeV gamma-ray detected in the YAP detector stopping it; and, the second, prompt, time-correlated gamma-ray pairs emitted from the source being detected in coincidence in the NE-213 and YAP detectors.

3. Results

3.1. Pulse Shape

The mixed neutron gamma field from the AmBe source was used to establish the pulse-shape discrimination (PSD) between electrons and protons and to measure the light yield dependent figures-of-merit (FOM). The detector signal was split into two independent signals and the current of each signal was integrated independently in the SG QDC and the LG QDC with 60 ns and 500 ns integration gate respectively (see Fig.4). The light yield difference of gamma induced recoiling electrons and of neutron induced recoiling protons is measured in a so-called "tail-to-total" charge comparison method by defining

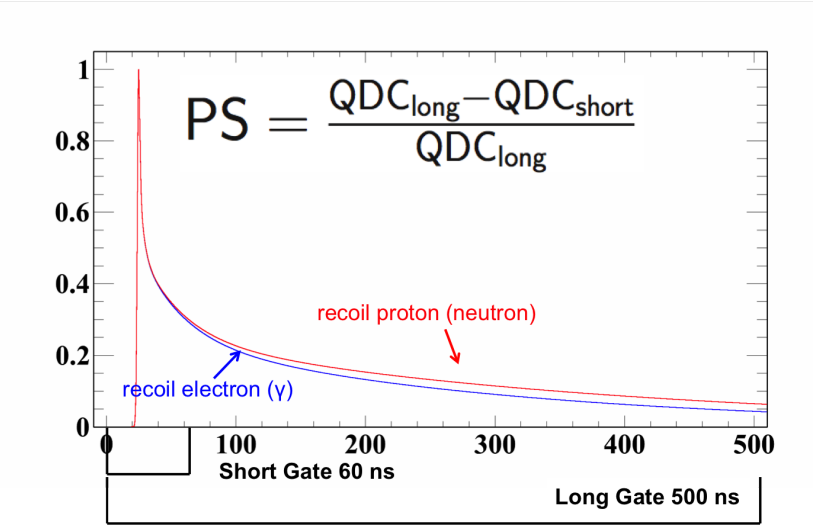

Figure 4: Light Pulse

a pulse-shape function (PS): the difference of the charges measured by the LG QDC and the SG QDC, normalized to the LG QDC charge:

$$\mathrm{PS} = \frac{\mathrm{QDC_{LG}} - \mathrm{QDC_{SG}}}{\mathrm{QDC_{LG}}} \tag{1}$$

It is well documented for liquid scintillators, that the PS of a light pulse is heavily influenced by the ionizing particle [26]. This is explained by an increase of the excitation of the long lived triplet state T_1 for particles with a high ionization density. T_1 is the main contributing factor to the slow decay component of a liquid scintillator via the bimolecular interaction of two molecules in the T_1 state to one molecule in the first singlet state S_1 and one in the ground state S_0. A direct result of this intrinsic liquid scintillator behavior is that the tail of an electron light pulse represents a smaller fraction of the whole light pulse than the tail of a proton pulse.

The integrated PS spectra is shown in fig. 5 for all light pulses with a light yield of 0.58 $\mathrm{MeV_{ee}}$ and higher. Two peaks can be identified in the histogram. The peak below PS=0.2 is corresponding to gamma induced recoiling electrons

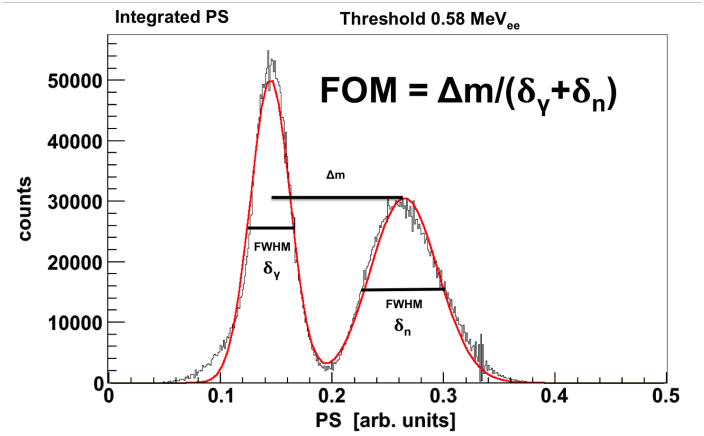

Figure 5: The integrated PS plot for all light yields larger than 0.58 MeV_{ee} is shown. A double gaussian function is fitted in red to the measured data. The FHWM of the Gaussian fits $\delta_{n,\gamma}$ and the position of the means $m_{n,\gamma}$ are clearly indicated. The FOM described in the plot will be discussed below.

and the peak at around PS=0.27 is corresponding to neutron induced recoiling protons. The FOM=1.03 of the detector for a 0.58 MeV_{ee} pulse height threshold can be easily calculated by the following equation:

$$\mathrm{FOM} = \frac{|m_n - m_\gamma|}{\delta_n + \delta_\gamma} \tag{2}$$

3.2. PSD

Figure 6 shows the deposited energy in the detector as a contour plot of PS over the light yield in electron equivalent energies L. The charge deposited in the SG QDC is directly proportional to the production of scintillation light by an electron. The excellent discrimination between neutron and gamma events is apparent for L > 0.5 Mev_{ee}. A small overlap exists between the two distributions below this threshold in the vicinity of PS = 0.2. The plot shows clearly that the strength of the PSD and therefore the FOM are strong functions of the light yield. To illustrate this fact four PS plots in blue corresponding to 1 MeV_{ee}, in red corresponding to 2 MeV_{ee}, in violet corresponding to 3 MeV_{ee}

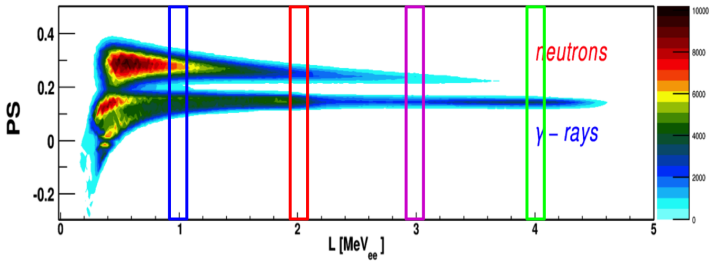

Figure 6: The figure shows the contour plot of PS over the light yield L. The detector shows an excellent separation above 0.5 M_{ee} and only small overlap in the region of PS = 0.2 below this threshold.

and in green corresponding to 4 MeV_{ee} have been drawn in fig. 7. It can be observed that the FWHM of the both the gamma and the neutron resolutions are decreasing for higher light yields. A second important feature of the detector for light pulse below 2.2 MeV_{ee} is apparent. The PS gamma distribution for those energies cannot be describe by a single Gauss distribution. We choose to fit those data as double Gaussian distributions instead.

3.3. FOM

Differential figures-of-merit were established by dividing the PSD plot into light yield intervals of an equal width of 0.1 MeV_{ee}. The FOM were determined by Gaussian fits. Below 2.2 MeV_{ee} the FOM has been calculated by fitting a double Gaussian function to the gamma distribution and a Gaussian function to the neutron distribution. For all other pulse heights single Gaussian functions were fitted to both the gamma and the neutron distributions. The PSD improves for higher light yields and the differential FOM is expected to increase with the light yield as discussed in the previous section.

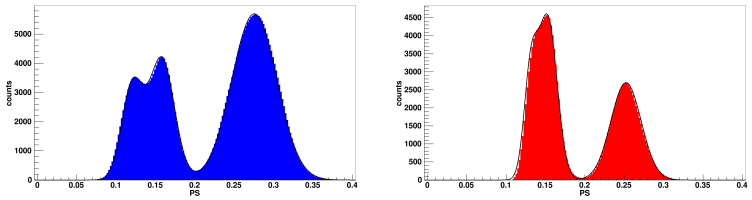

(a) Pulse shape distribution for pulse with a light yield of 1 MeV_{ee}.

(b) Pulse shape distribution for pulse with a light yield of 2 MeV_{ee}.

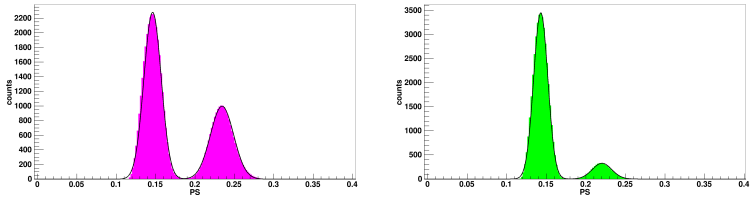

(c) Pulse shape distribution for pulse with a light yield of 3 MeV_{ee}.

(d) Pulse shape distribution for pulse with a light yield of 4 MeV_{ee}.

Figure 7: PS plots for different pulse heights.Gaussian fits have been applied in black.

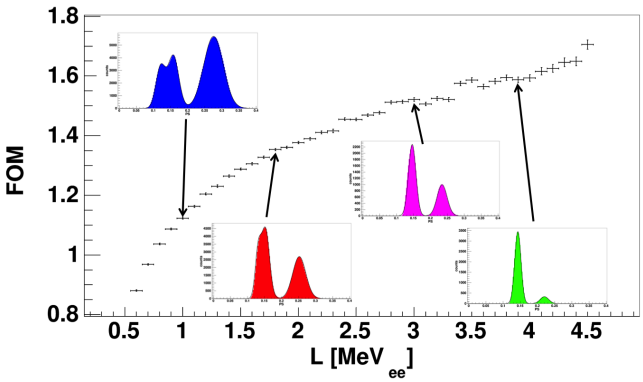

Figure 8: The differential FOM over the light yield L.

3.4. Proton Light Yield

In a second step, the TOF of neutron events was used to determine the kinetic energy of the tagged neutrons in the detector [13] and the random neutron background was subtracted from the pulse height/light yield spectrum. Figure 9 shows the TOF spectra of the measurement. The top panel, a contour plot of the PS over the TOF, shows the correlation between particle species, in both TOF and PS. Neutrons can be easily identified by both TOF and PS. In the middle of Figure 9 the neutron (shaded in red) and gamma (non shaded in blue) TOF spectra are shown. The bottom panel shows the neutron pulse height plotted over the TOF in a contour plot. It is obvious that the maximum light yield of neutron induced recoiling protons is a strong function of the kinetic energy of the incident neutrons. The events in the two lower panels were chosen by applying the PSD established above. The proton light yield was determined by creating pulse height histograms for incident neutron energies in intervals of 0.2 MeV. In a perfect detector system the sharp edge of those histograms is identical with total energy transfer from an incident neutron to a recoiling proton. In our detector the edge is smeared by resolution effects. Two different methods were applied to calculate the edge. The first way was to apply the Knox method normally used to determine the Compton edge of incidence gamma rays to the neutron edge. The second method was to find the the high energetic minimum of the first derivative of the light yield function L as suggested in [12] (in the future revered to as the Kornilov method). The derivative was calculated from the smoothed functions with a simple numeric derivation algorithm. Figure 10 show both the neutron response function for 5.8 MeV incidence neutrons and the first derivative of the function.

The non linearity of the proton light yield L_p of liquid scintillators in general and NE-213 in particular has been reported. In the past the empirical method of Madey [27] was applied wildly. We decided to use the more recently suggested method of Kornilov et al. [12].

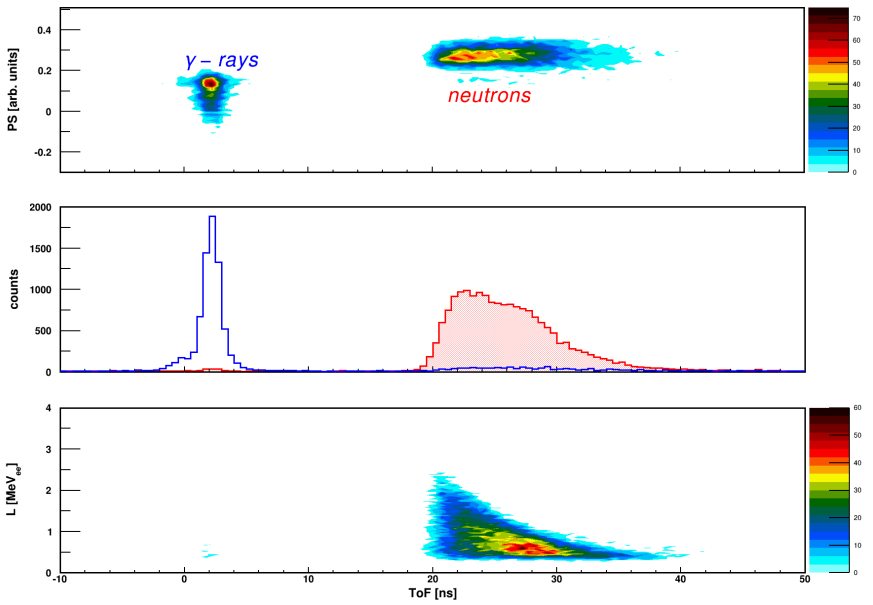

Figure 9: The top panel shows the contour plot of the PS over the time-of-flight. A strong correlation between particle species and TOF is clearly visible. The central panel shows the time of flight spectra for events identified by PSD as gammas in the non-shaded (blue) histogram and neutron events shaded in red. The sharp distribution in the blue histogram around 2 ns is the so-called γ-flash. In the bottom panel we see the contour plot of the light yield L over the TOF for neutron events identified by PSD. The decrease of the maximum light yield for the neutron events from 20 ns TOF to 40 ns TOF indicates a strong correlation between neutron energy and maximum light yield.

Scintillator		L_0	L_1
NE-213	This Work with Kornilov Method	0.615 ± 0.028	2.92 ± 0.29
NE-213	This Work with Knox Method	0.609 ± 0.051	2.97 ± 0.61
NE-213	Naqvi	0.620 ± 0.035	3.07 ± 0.42
SL301	Kornilov	0.579 ± 0.008	2.41 ± 0.11
BC501A	Kornilov	0.642 ± 0.012	2.96 ± 0.15

Table 1: A list of the proton light yield parametrization for NE-213 after Kornilov et al. [12].

$$L_p = L_0 \frac{T_n^2}{T_n + L_1} \tag{3}$$

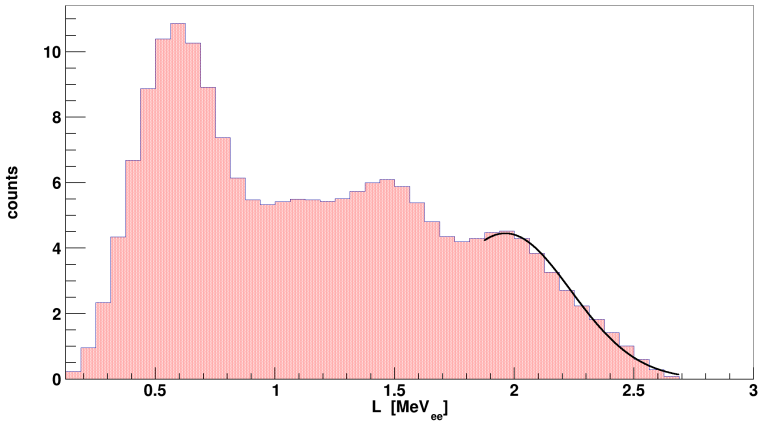

Figure 10: The light yield L in electron equivalent energies for 5 MeV neutrons.

Figure 11 shows the proton light yield for NE-213 from this work as gray filled squares in the top panel (Knox method) and as gray filled circles in the middle panel (Kornilov method). The results for an SL301 provided by Scinonix [16] (h =50 mm x d = 100 mm) from [12] are shown as open (red) circles in the middle. In the top panel the data of Naqvi et al. [11] for a NE-213 detector of 50 mm x 50 mm is shown as open squares (blue). It is important to member that

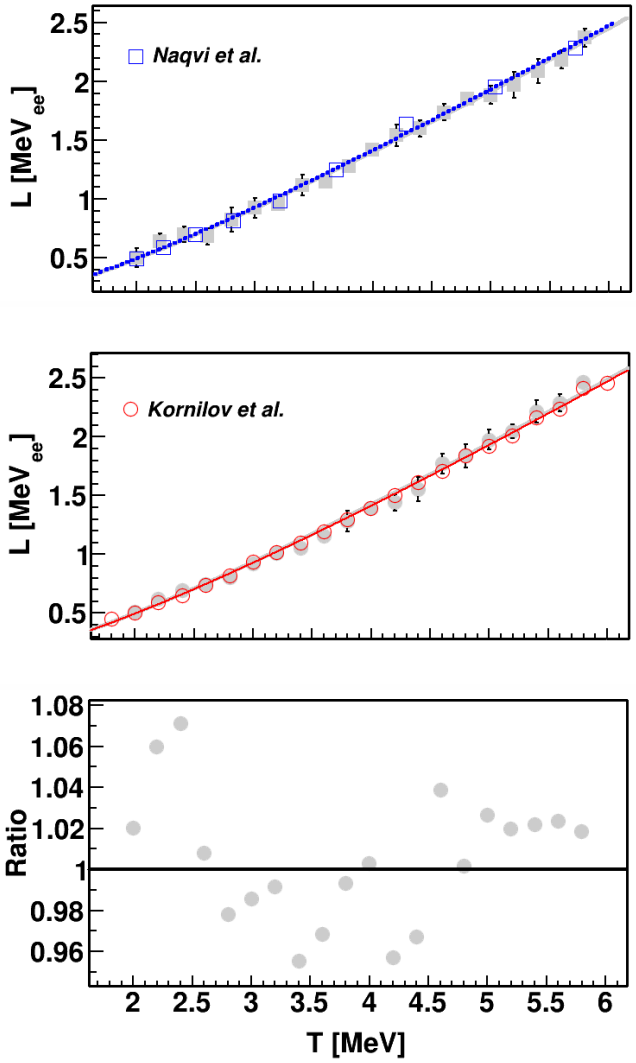

Figure 11: The top panel shows the proton light yield determined with the Knox method over the kinetic energy as gray filled squares and the values from Naqvi et al. [11] as open blue squares. In the middle the filled circles (gray) are the results from this work calculated with the Kornilov method. The open (red) circles is data taken from [12]. The bottom panel shows the ratio of L Kornilov over L Knox.

the Naqvi data was also determined by fitting a Gaussian distribution to the edges of the neutron response functions, while the Kornilov data was computed by calculating the first derivatives of the the response functions. The bottom panel shows the ratio of our data calculated with the Kornilov method over our data from the Knox method. The data shows a good agreement and does diverge less than 10% for all measured energies and on average about 1%. The comparison of our data to the Kornilov data yields similarly results. A point by point comparison to the Naqvi data was not possible, since Naqvi et al. chose to not divided their TOF spectra into equal energy intervals, but used single TDC channels instead. The excellent agreement with our results is still obvious. In a next step, we fitted equation 3 with a least-square method to our data and the data taken from [11]. In table 1 the fitting results for those three data samples are listed together with the results from Kornilov for both the LS301 detector and for a BC501A [14] detector (h = 25 mm x d = 100 mm). Both parameters L_0 and L_1 are in good agreement or atleast within the calculated errors for all samples with the exception of the SL310 sample. However, if the SL310 data is fitted in the same energy range as our measurement for incidence neutrons from 2 MeV up to 5.8 MeV, we could not recalculate the lower values for the SL310 scintillator. With data taken from a figure in [12] with the software Plot Digitizer [28], we computed the following values for $L_0 = 0.617 \pm 0.013$ and $L_1 = 3.02 \pm 0.17$ respectively.

4. Conclusion

The in-depth analysis of the fast neutron reference detector demonstrates a cost efficient way to characterize fast neutron detectors in an energy range between 2 MeV and 6 MeV with an AmBe source. We determined the differential PS functions for light yields of up to $L = 4.6\ MeV_{ee}$. We used the neutron/gamma PSD and the TOF to establish NE-213 neutron response functions and to discriminate against any random gamma background. We tested two widely applied methods to calculate the proton light yield in electron equiv-

alent energies. Both those methods agree better than 10% with each other. The same is true, if our results are compared to previous source based measurements with both an AmBe source [11] and a ^{252}Cf source [12].

Acknowledgments

We thank the Photo-Nuclear group at MAX IV laboratory to providing us access to their facility. We acknowledge the support of the UK Science and Technology Facilities Council, as well as the the support of the Royal Physiographic Society in Lund.

References

[1] United States Committee on Army Science and Technology for Homeland Defense, Board on Army Science and Technology, Division on Engineering and Physical Sciences, National Research Council, Indications and Warning Technologies, in Science and Technology for Army Homeland Security: Report 1, National Academies Press (2003).

[2] W. Lyons, G. Plisga, Current practice in well logging, reservoir engineering and secondary recovery. In: The Petroleum Engineering Handbook: Sustainable Operations, Gulf Publishing Company, 2013.

[3] R. Chandra, et al., IEEE NSS/MIC (2010) 508.

[4] M. Islam, M. Kahn, Drilling and well completions, reservoir engineering. In: Standard Handbook of Petroleum and Natural Gas Engineering, Gulf Publishing Company, 2011.

[5] A. Tomanin, et al., Nucl. Inst. and Meth. A 756 (0) (2014) 45.

[6] J. Walker, Phys. Technol. 13 (1982) 239.

[7] R. Chandra, et al., J. Instrum. 7 (2012) C03035.

[8] C. Bass, et al., App. Rad. and Isot. 77 (2013) 130.

[9] A. Horváth, et al., Nucl. Inst. and Meth. A 440 (1) (2000) 241.

[10] M. Aspinall, et al., Nucl. Inst. and Meth. A 583 (2–3) (2007) 432 – 438.

[11] A. Naqvi, et al., Nucl. Inst. and Meth. A 353 (1994) 156–159.

[12] N. Kornilov, et al., Nucl. Inst. and Meth. A 599 (2009) 226.

[13] J. Scherzinger, et al., App. Rad. and Isot. 98 (2015) 74.

[14] NE213 is no longer produced. Eljen Technologies offers EJ-301 (http://www.eljentechnology.com/index.php/products/liquid-scintillators/71-ej-301) while Saint Gobain offers BC-501 (http://www.crystals.saint-gobain.com/uploadedFiles/SG-Crystals/Documents/SGC%20BC501_501A_519%20Data%20Sheet.pdf).

[15] Supplied by High Tech Sources Limited, Unit 6, Moorbrook, Southmead, Industrial Estate, Didcot, Oxfordshire, Uk OX11 7HP; http:///www.hightechsource.co.uk/. For details see http:///www.hightechsource.co.uk/Legacy/Resources/Americium-Berryliu.pdf. .

[16] (The linke seems to be broken!!! One can still access other sides but the homepage seems to be gone. !!!!! Scionix Holland BV. http://www.scionix.nl).

[17] (Hamamatsu Photonics. http://www.hamamatsu.com).

[18] (http:///www.eljentechnology.com/index.php/products/paints/87-ej-520).

[19] (http://www.huntsman.com/advanced_materials/a/Our%20Technologies/Ready%20to%20Use%20Formulated%20Systems/Adhesives).

[20] (http://www.us.schott.com/borofloat/english/index.html for details. Supplied by Glasteknik i Emmaboda AB, Utv agen 6 SE-361 31 Emmaboda, Sweden.).

[21] Viton is a registered tradmark of DuPont Perfomrance Elastomers LLC.

[22] (Supplied by Nordic Plastics Group AB, Bronsyxegatan 6, SE-213 75 Malmö, Sweden).

[23] (http:///www.eljentechnology.com/index.php/products/paints/87-ej-510).

[24] (E T Enterprise Ltd. http://www.et-enterprises.com).

[25] H. Knox, T. Miller, Nucl. Inst. and Meth. 101 (1972) 519.

[26] G. Knoll, Radiation detection and measurement, John Wiley and Sons, (1989).

[27] R. Madey, et al., Nucl. Inst. and Meth. 151 (3) (1978) 445.

[28] (http://plotdigitizer.sourceforge.net/).

The project reported upon in this thesis
was performed in collaboration with

The Source-based Neutron Irradiation Group
of the Division of Nuclear Physics at Lund University

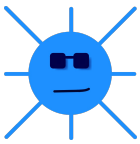

and the

The Detector Group of the European Spallation Source